Fermi National Accelerator Laboratory

FERMILAB-Pub-76/40-THY
May 1976

Neutrino-Proton Elastic Scattering: Implications for Weak Interaction Models

CARL H. ALBRIGHT*, C. QUIGG†, R. E. SHROCK
and J. SMITH§
Fermi National Accelerator Laboratory**
P.O. Box 500, Batavia, Illinois 60510

ABSTRACT

We test the predictions of various gauge models for weak neutral current interactions by comparing them with experimental results on inclusive and elastic neutrino interactions. The Weinberg-Salam model is in fair agreement with the data; however, vector-like theories can be ruled out. We also consider certain gauge models with five or six quarks and one or two right-handed doublets, and find that they fit the data rather well.

---

* Permanent address: Department of Physics, Northern Illinois University, DeKalb, Illinois 60115; work supported in part by National Science Foundation Grant No. MPS 75-05467.

† Supported in part by the Alfred P. Sloan Foundation; also at Enrico Fermi Institute, University of Chicago, Chicago, Illinois 60637.

§ Permanent address: Institute for Theoretical Physics, State University of New York, Stony Brook, New York 11794; work supported in part by National Science Foundation Grant No. GP-32998X.

** Operated by Universities Research Association, Inc., under contract with the U. S. Energy Research and Development Administration.

I. INTRODUCTION

The discovery of neutral currents in neutrino-induced reactions[1] has led to major revisions in our understanding of the weak interactions. While it can be argued that a theoretical framework (Yang-Mills gauge field theory with spontaneous symmetry breaking[2]) already existed to incorporate the neutral current, it is still not clear which model, if any, will survive. Measurements of neutral current phenomena[3] are extraordinarily difficult, so it has been necessary to interpret with caution quantitative results from the first generation "discovery" experiments. However, new experiments are in progress which promise ultimately to give reasonably precise information and to allow discrimination among theoretical models.

Until now, testing of models has relied principally upon values or upper limits for integrated neutral current cross sections. Although this information provides an important first test of the consequences of models, differential distributions make more stringent demands upon candidate theories. Fortunately, differential cross sections are now being measured for a variety of neutral current processes.

The experiments which have revealed new structure in the weak interaction fall into six major categories.

(A). Inclusive neutrino and antineutrino interactions on approximately isoscalar nuclear targets:

$$\nu + N \rightarrow \nu + X , \tag{1.1a}$$

$$\bar{\nu} + N \rightarrow \bar{\nu} + X. \tag{1.1b}$$

The first evidence for "muonless" events[1] came from these reactions. Experimental results are usually presented in terms of the ratio of the neutral current cross section to the charged current cross section, namely

$$R^{\nu N} = \sigma(\nu + N \rightarrow \nu + X)/\sigma(\nu + N \rightarrow \mu^- + X) \tag{1.2a}$$

$$R^{\bar{\nu}N} = \sigma(\bar{\nu} + N \rightarrow \bar{\nu} + X)/\sigma(\bar{\nu} + N \rightarrow \mu^+ + X), \tag{1.2b}$$

where N denotes an isoscalar target.

The most recent experimental results are given in Ref. 4. Indications are that the effective form of the charged current (and conceivably also that of the neutral current) is changing at high energies,[5] presumably due to the activation of new quarks and right-handed currents. These new effects seriously complicate discussions of the neutral current in terms of the ratios $R^{\nu N}$ and $\bar{R}^{\bar{\nu}N}$, which contain charged current cross sections in the denominator.

(B). Inclusive reactions on proton targets:

$$\nu + p \rightarrow \nu + X, \tag{1.3a}$$

$$\bar{\nu} + p \rightarrow \bar{\nu} + X. \tag{1.3b}$$

Preliminary data on these reactions are now available.[6]

(C). Single pion production in neutrino and antineutrino interactions, either on isoscalar targets or on free protons[7]:

$$\nu + N \rightarrow \nu + \pi + N \qquad (1.4)$$

These channels are of key importance in the determination of the isospin content of the weak neutral current. The experimental situation has been somewhat confused on this point, but recent results from Argonne, Brookhaven, and CERN indicate that both isoscalar and isovector currents are present.[8]

(D). Inclusive production of specific final states, such as $\Delta S = -\Delta Q$ events, or $\mu^- e^+$ events induced by incident neutrinos.[9] Bubble chamber data on other specific final states are already available from the Gargamelle chamber at CERN and from Fermilab.[10]

(E). Elastic neutrino and antineutrino scattering from protons:

$$\nu + p \rightarrow \nu + p, \qquad (1.5a)$$

$$\bar{\nu} + p \rightarrow \bar{\nu} + p. \qquad (1.5b)$$

The first positive evidence for the neutrino reaction has just been published by a Columbia-Illinois-Rockefeller collaboration and a Harvard-Pennsylvania-Wisconsin collaboration, both working at Brookhaven.[11] The HPW group has also reported observation of the antineutrino reaction.[11]

(F). Purely leptonic processes, such as the elastic scattering of neutrinos by electrons:

$$\nu_\mu + e \rightarrow \nu_\mu + e, \quad \text{etc.} \tag{1.6}$$

The present status of these reactions has been reviewed by Faissner.[12] The purely leptonic reactions, being free from the influence of the strong interactions, are the most easily interpreted of the neutral current phenomena. All the models considered here, once having specified the behavior of the weak current in the lepton sector, make unambiguous predictions for them--provided the ratio of the neutral and charged intermediate boson masses is uniquely determined by the mixing angle.

We have nothing to add to previous discussions regarding categories (C), (D), and (F). However, with the appearance of measurements of the elastic reaction (E), revised and extended data on the deep-inelastic reactions (A), and preliminary results on the deep-inelastic reactions (B), it seems appropriate to undertake an analysis of these experimental results in the context of certain popular theoretical models. In so doing, we shall limit our analysis to models based on gauge theories having only vector and axial vector currents. We shall not consider models which incorporate scalar, pseudoscalar, or tensor interactions.[13] The status of such unconventional models has been assessed in a recent report by Fischbach, et al.[14]

The logical structure of our analysis is as follows. First we attempt to fit the data on inclusive reactions with isoscalar targets. We do this not to rule out any models, but rather to fix parameters. Using these constraints we predict the inclusive cross sections for proton targets and the differential cross sections for elastic scattering. The predictions of the various models are then compared with recently published results.

On the basis of the elastic scattering data now available we can draw the following tentative conclusions. The Weinberg-Salam model[2] is in good agreement with the shape of the differential cross sections for both the νp and $\bar{\nu}p$ reactions. It also agrees well with the total $\bar{\nu}p$ cross section but predicts a value for $\sigma^{\nu p}$ which is about one and a half standard deviations below what is observed. Six quark vector models[15] appear to be inconsistent with the shape of the νp differential cross section. A five-quark model due to Achiman, Koller, and Walsh[16] (which is essentially equivalent to a six-quark model introduced by Fayet[17] and Barnett[17]) and two variants of the Gürsey-Ramond-Sikivie model[17] satisfactorily account for the observed νp and $\bar{\nu}p$ data in shape and magnitude. The sensitivity of these conclusions to assumptions on the behavior of nucleon form factors will be discussed below.

The rest of this article is divided into several sections. Examples of gauge field theory models are given in section II. Our review of the models is quite brief; we refer the reader to the original papers for details and motivation. Our chief aim here is to establish notation and list the couplings required for subsequent calculations. Section III contains a discussion of inclusive cross sections for neutrino- and antineutrino-nucleon scattering. We employ a quark-parton model framework for this analysis,

and include a brief description of the model. In addition, we deal briefly with the problem of rescaling above the thresholds for new-particle production. The elastic scattering of (anti)neutrinos from nucleons occupies Sec. IV. We give results for both reactions although the available data are for neutrino beams only, in anticipation of the corresponding measurements for antineutrinos. Finally, in Sec. V we state our conclusions.

II. GAUGE MODELS

Many renormalizable gauge theory models exist which make reasonably well-defined predictions for weak neutral current reactions. In the models which are simplest and most amenable to experimental test, the weak and electromagnetic interactions are described by the gauge group $SU(2)\otimes U(1)$. In this paper we consider several of the popular theories in this class. The general characteristics of these gauge theory models are by now well known and will not be reviewed again here, except for the purpose of establishing notation.

Corresponding to the four generators of the group $SU(2)\otimes U(1)$ are the four gauge fields $W_\mu^a (a = 1, 2, 3)$, and B_μ. After the symmetry is spontaneously broken by means of the Higgs mechanism, the resulting mass eigenstates are the intermediate vector bosons $W_\mu^\pm$, Z_μ^0, and the photon A_μ. These fields are coupled in a minimal gauge-covariant manner to the fermion fields. In the models to be considered here the quarks

and leptons are placed in left-handed and right-handed multiplets which transform under weak SU(2) as singlets or doublets.

The gauge coupling constants g and g' (for the SU(2) and U(1) groups, respectively) are constrained by a single relation involving the electromagnetic coupling constant e. For the Weinberg-Salam (W-S) model[2] the constraint is

$$e = g\,g'/(g^2 + g'^2)^{\frac{1}{2}} \quad . \tag{2.1}$$

Thus there is only one independent parameter,[18] which is conventionally taken to be the Weinberg angle, defined by

$$\tan\theta_W = g'/g. \tag{2.2}$$

In the simplest realization of spontaneous symmetry breaking one uses a complex doublet of Higgs scalars and there results a relation between the masses of the $W^{\pm}$ and Z^0:

$$\frac{g^2 + g'^2}{M_Z^2} = \frac{g^2}{M_W^2} \quad , \tag{2.3a}$$

i.e.

$$M_W/M_Z = \cos\theta_W \quad . \tag{2.3b}$$

In a more general Higgs scheme, however, the mass ratio is arbitrary, and Eq. (2.3a) becomes

$$\frac{g^2 + g'^2}{M_Z^2} = \kappa \frac{g^2}{M_W^2} . \tag{2.4}$$

As a consequence, the weak neutral current cross section is scaled by the factor κ^2 relative to its charged current counterpart.

Let us next describe the fermion content of the various theories. The relevant[19] part of the lepton sector is common to them all: the usual leptons are arranged in two left-handed doublets $\begin{pmatrix} \nu_e \\ e \end{pmatrix}$ and $\begin{pmatrix} \nu_\mu \\ \mu \end{pmatrix}$. In the hadron sector, the Weinberg-Salam model[2] with the obligatory Glashow-Iliopoulos-Maiani modification to avoid strangeness changing neutral currents[20] involves four flavors of colored quarks, u, d, s, c. These are arranged in two left-handed doublets as shown in Table I. The Cabibbo-rotated quarks are given by

$$\begin{aligned} d_\theta &= d \cos\theta_C + s \sin\theta_C \\ s_\theta &= -d \sin\theta_C + s \cos\theta_C , \end{aligned} \tag{2.5}$$

where θ_C is the Cabibbo angle.

The Weinberg-Salam model has fared reasonably well in its predictions for neutral current phenomena. It may also be able to explain the dimuon production in neutrino and antineutrino experiments.[5] However

it cannot account for the anomalous $d\sigma_{cc}^{\bar{\nu}}/dy$ distributions or for the increases in $\langle y \rangle^{\bar{\nu}}$ and $R_{ch} = \sigma_{cc}^{\bar{\nu}}/\sigma_{cc}^{\nu}$ observed in high-energy (anti)neutrino charged current (cc) reactions.[5]

One plausible explanation of these results hypothesizes the production of new quarks by right-handed currents and, consequently, physical hadrons with new quantum numbers beyond charm. An appealing model based on this observation was introduced by several groups.[15, 21] In this model there are six quark flavors: three charge +2/3 quarks u, c, t, and three charge -1/3 quarks d, s, b. These are assigned symmetrically to three left-handed and three right-handed doublets, as shown in Table 1.

It is important to observe that the structure of the quark assignments in this model is essentially unique, up to small mixing angles, once the choice is made to place all quarks in doublets. It is necessary to have the $\binom{c}{s}_L$ doublet in order to avoid strangeness-changing neutral currents in lowest order. The left-handed t and b quarks must then be put in the same doublet $\binom{t}{b}_L$. Among the right-handed doublets, $\binom{u}{d}_R$ and $\binom{u}{s}_R$ cannot occur since this would contradict low energy meson and hyperon decay data which show that $\Delta S = 0$ and $\Delta S = 1$ weak decays are V-A. Furthermore, one cannot place the right-handed c and d quarks in the

same doublet, as $\binom{c}{d}_R$, since this would predict[22] the wrong relative signs of the $\Delta I = 1/2$ and $\Delta I = 3/2$ amplitudes in the decays $K \to 2\pi$ and $K \to 3\pi$. In addition it could lead to too large a $K_L - K_S$ mass difference.[23] One is thus forced to arrange the right-handed quarks as $\binom{u}{b}_R$, $\binom{c}{s}_R$, and $\binom{t}{d}_R$, again up to small admixtures. This model is vector-like in the sense that the neutral current is pure vector while the charged current becomes pure vector in the asymptotic energy region far above thresholds for new flavor production.

It is of interest to compare this model with the $\nu p \to \nu p$ scattering data, independent of its predictions for inclusive reactions. However it must be remarked that this theory is already in conflict with the latter data. Although it can account for the high y anomaly and growth in $\langle y \rangle^{\bar{\nu}}$ and R_{ch}^{ν} it predicts (unless one makes the mass of the t quark huge) that σ_{cc}^{ν}/E should increase by a factor of $\sim \frac{4}{3}$ and $\frac{d\sigma_{cc}}{dy}$ should change from ~ 1 to $(1 + (1 - y)^2)$. These features do not seem to be observed in the charged current data. More seriously, the inclusive data rule out a purely vector neutral current.[24]

Accordingly, we shall also consider a third class of models in which a t quark does not appear and the neutral current is parity violating. Probably the simplest albeit rather asymmetric model, proposed by Achiman, Koller and Walsh,[16] involves five quark flavors. In this model the fifth quark, called b, has $Q = -1/3$ and is placed in a single right-handed doublet $\binom{u}{b}_R$. We shall actually consider a generalization of the model in which the right-handed doublet is $\binom{u\ \phi}{b}_R$, as shown in Table 1.

A class of models which gives quite similar predictions has been proposed by Fayet[17], by Barnett[17] and by Gürsey, Ramond and Sikivie.[17] These models contain six quarks, which are arranged in two left-handed and two right-handed doublets. For our calculations we shall concentrate on versions (B) and (C) of the Gürsey-Sikivie model, for which the quark doublets are shown in Table 1. The $Q = -1/3$ quarks in the $V + A$ sector are rotated according to

$$b_{\phi R} = b_R \cos\phi + b'_R \sin\phi \tag{2.6}$$

and

$$b'_{\phi R} = -b_R \sin\phi + b'_R \cos\phi$$

with $b'_{\phi R}$ being the singlet. In the G-S model (C), the u and c quarks are rotated in the left-handed doublet according to

$$u_{\alpha L} = u_L \cos\frac{\alpha}{2} + c_L \sin\frac{\alpha}{2}$$
$$c_{\alpha L} = -u_L \sin\frac{\alpha}{2} + c_L \cos\frac{\alpha}{2} \ , \tag{2.7}$$

while the following rotated left-handed $Q = -1/3$ quarks also appear in doublets (see Table I)

$$d_{\alpha L} = d_L \cos\frac{\alpha}{2} + b_L \sin\frac{\alpha}{2}$$
$$b'_{\alpha L} = -s_L \sin\frac{\alpha}{2} + b'_L \cos\frac{\alpha}{2} \ . \tag{2.8}$$

In the (C) version, $\tan^2 \frac{\alpha}{2} = \tan \theta_C$, so the d → c transition is suppressed by only $\tan \theta_C$ rather than $\tan^2 \theta_C$. Moreover, cancellation of the cross terms does not occur via a GIM mechanism with the result that above b and b' thresholds, the neutral current becomes flavor-changing.

We complete this section by noting the general structure of the charged and neutral currents in these SU(2) ⊗ U(1) gauge models. The charged current has the form

$$J_\mu^{(\pm)} = \sum_L \bar{\psi}_L \tau_\pm \gamma_\mu (1 + \gamma_5) \psi_L + \sum_R \bar{\psi}_R \tau_\pm \gamma_\mu (1 - \gamma_5) \psi_R \qquad (2.9)$$

where the first sum runs over the left-handed doublets and the second one over the right-handed doublets, if any. The weak neutral current is

$$J_\mu^{(0)} = \frac{1}{2} \sum_L \bar{\psi}_L \tau_3 \gamma_\mu (1 + \gamma_5) \psi_L + \frac{1}{2} \sum_R \bar{\psi}_R \tau_3 \gamma_\mu (1 - \gamma_5) \psi_R \qquad (2.10)$$

$$- 2 \sin^2 \theta_W J_\mu^{em} ,$$

in terms of the electromagnetic current

$$J_\mu^{em} = \frac{2}{3} \sum_{Q_i = 2/3} \bar{q}_i \gamma_\mu q_i - \frac{1}{3} \sum_{Q_i = -1/3} \bar{q}_i \gamma_\mu q_i . \qquad (2.11)$$

For use in Section IV, we note that the neutral currents in the u-d space can be decomposed into isoscalar and isovector U(2) components according to

$$J_\mu^{(0)} = \alpha V_\mu^3 - \beta A_\mu^3 + \frac{1}{3}\gamma V_\mu^0 - \delta A_\mu^0$$

$$J_\mu^{em} = V_\mu^3 + \frac{1}{3}V_\mu^0 \quad . \tag{2.12}$$

The four parameters of each model are listed in Table II.

III. INCLUSIVE NEUTRAL CURRENT REACTIONS

We shall next calculate the ratios $R^{\nu N}$, $R^{\bar{\nu}N}$, $R^{\nu p}$, and $R^{\bar{\nu}p}$ predicted by the gauge models discussed in the previous section. Comparing the ratios for reactions on isoscalar targets with the data, we determine for each model a value of $\sin^2\theta_W$ which yields optimal agreement. These values will then be used in the analysis of the elastic reactions.

We must note that there is inherent in this method a certain problem caused by the new phenomena which appear at high energies in the inclusive charged current reactions. The ratios R^{ν} and $R^{\bar{\nu}}$ are independent of energy only in the low energy region below charm threshold. However, the Harvard-Pennsylvania-Wisconsin-Fermilab (HPWF) and the Caltech-Fermilab (CITF) experiments probe an energy range well above the Brookhaven and CERN energies of a few GeV. For example, the HPWF group quotes[4] a value of E = 41 GeV as the average energy (after a cut in W) of the events used in their measurement of $R^{\bar{\nu}N}$. Since the data indicate that $(\sigma_{cc}^{\bar{\nu}N}/E)$ is increasing with energy in this region, whereas

($\sigma_{nc}^{\bar{\nu}N}/E$) is presumably constant (as is ($\sigma_{nc}^{\nu N}/E$)), one would expect the measured values of $R^{\bar{\nu}N}$ to be somewhat lower than the same quantity measured at Brookhaven and CERN energies. Unfortunately, the present data are not precise enough to confirm this expectation. Hence we do not think it appropriate to try to make a correction to the Fermilab data to obtain values of $R^{\bar{\nu}N}$ which are supposedly more applicable to the Gargamelle data. We shall, however, give results showing the energy dependence of R^{ν} and $R^{\bar{\nu}}$ for the models studied. Given the size of the error bars on the data, our determination of the optimal value of $\sin^2\theta_W$ for each model is only approximate; at this stage it is thus not too sensitive to the energy dependence of R^{ν} and $R^{\bar{\nu}}$.

The differential cross section for the inclusive neutrino reaction $\nu(\bar{\nu})N \to \mu^{\mp} X$ is

$$\frac{d^2\sigma(\nu,\ \bar{\nu})N}{dxdy} = \frac{G^2ME}{\pi}\left[xy^2F_1^{(\nu,\ \bar{\nu})N} + (1-y)F_2^{(\nu,\ \bar{\nu})N} \mp y(1-\frac{y}{2})xF_3^{(\nu,\ \bar{\nu})N}\right] \quad (3.1)$$

where $x = Q^2/2M\nu$ and $y = \nu/E$ are the usual scaling variables and N denotes an isoscalar target. The same equation applies, with appropriate changes in the structure functions, to the charged current reactions $\nu(\bar{\nu})p \to \mu^{\mp} X$ and the neutral current reactions $\nu(\bar{\nu})N \to \nu(\bar{\nu})X$ and $\nu(\bar{\nu})p \to \nu(\bar{\nu})X$. When a heavy quark is produced in the quark transition $q_i(+W^{\pm}) \to q_j$ the variable x is no longer equal to the fraction of the total

proton momentum carried by the initial quark q_i. Rather, this fraction is equal to[25]

$$z_j = x + \frac{m_j^2}{2ME_y} \tag{3.2}$$

where m_j is the effective mass of the final quark q_j. Of course in light quark → light quark transitions z_j reduces to x. The Callan-Gross relation for the allowed transitions $q_i \to q_j$ or $\bar{q}_i \to \bar{q}_j$ is

$$F_2(z_j) = 2\, z_j F_1(z_j) \tag{3.3}$$

Similarly, the relation between F_2 and F_3 is

$$-z_j F_3(z_j) = \eta\, F_2(z_j) \tag{3.4}$$

where

$$\eta = \begin{cases} +1 \text{ for } (q_i)_L \to (q_j)_L \\ \quad \text{or } (\bar{q}_i)_R \to (\bar{q}_j)_R \\ -1 \text{ for } (q_i)_R \to (q_j)_R \\ \quad \text{or } (\bar{q}_i)_L \to (\bar{q}_j)_L \end{cases} \tag{3.5}$$

As an illustration of the calculation we list below the structure functions for the charged and neutral current neutrino reactions on an isoscalar target, in the six quark vector model:

$$F_{2,\,cc}^{\nu N} = x(u(x) + d(x))\cos^2\theta_C + x(\bar{u}(x) + \bar{d}(x)) + 2x\,s(x)\sin^2\theta_C$$
$$+ z_c\Theta_c\left\{\left(u(z_c) + d(z_c)\right)\sin^2\theta_C + 2s(z_c)(\cos^2\theta_C + 1)\right\} \qquad (3.6)$$
$$+ z_b\Theta_b\left(\bar{u}(z_b) + \bar{d}(z_b)\right) + z_t\Theta_t\left(u(z_t) + d(z_t)\right)$$

$$-F_{3,\,cc}^{\nu N} = (u(x) + d(x))\cos^2\theta_C - (\bar{u}(x) + \bar{d}(x)) + 2s(x)\sin^2\theta_C$$
$$+ \Theta_c\left\{\left(u(z_c) + d(z_c)\right)\sin^2\theta_C + 2s(z_c)(\cos^2\theta_C - 1)\right\} \qquad (3.7)$$
$$+ \Theta_b\left(\bar{u}(z_b) + \bar{d}(z_b)\right) - \Theta_t\left(u(z_t) + d(z_t)\right)$$

$$F_{2,\,nc}^{\nu N} = x\left[\frac{1}{2}\left\{\left(1 - \frac{4}{3}x_W\right)^2 + \left(-1 + \frac{2}{3}x_W\right)^2\right\}(u(x) + \bar{u}(x) + d(x) + \bar{d}(x))\right.$$
$$\left. + \left(-1 + \frac{2}{3}x_W\right)^2(s(x) + \bar{s}(x))\right] \qquad (3.8)$$

$$F_{3,\,nc}^{\nu N} = 0 \qquad (3.9)$$

In Eqs. (3.6) and (3.7) θ_C is the Cabibbo angle and Θ_j (j = c, b, t) is a theta function which vanishes unless the hadronic invariant mass W is greater than the threshold value associated with the production of a heavy quark of flavor j. In Eqs. (3.8) and (3.9), $x_W = \sin^2\theta_W$.

The parton distributions incorporate the conventional SU(3)-symmetric sea:

$$u(x) = u_v(x) + \xi(x) \tag{3.10a}$$

$$d(x) = d_v(x) + \xi(x) \tag{3.10b}$$

$$\bar{u}(x) = \bar{d}(x) = s(x) = \bar{s}(x) = \xi(x) \ , \tag{3.10c}$$

with other flavors absent. We use the Pakvasa-Parashar-Tuan parametrization,[26] which has a sea quark distribution $\xi(x) \propto x^{-1}(1 - x)^{7/2}$ and gives a representative description of the leptoproduction data. For comparison we have also used a parton distribution due to Field,[27] which also gives a satisfactory description of the leptoproduction data, but has a sea quark distribution $\xi(x) \sim x^{-1}(1 - x)^{7}$. The observables we consider here are insensitive to these differences.

The results of our calculations of $R^{(\nu,\ \bar{\nu})N}$ and $R^{(\nu,\ \bar{\nu})p}$ for the four types of models are shown in Figs. 1 through 10. These are to be compared with the data listed in Table III. These data come from the CERN Gargamelle experiment, and from the HPWF and CITF experiments at Fermilab. For the CERN results we have included both the published values and more recent values presented at the Rencontre de Moriond, 1976. For all three experiments the determination of $R^{\nu N}$ and $R^{\bar{\nu}N}$ involves important experimental cuts and corrections. It would be inappropriate to discuss these in detail here; we urge the reader to consult the original references.

It is of interest, however, to summarize the energies involved in these experiments. The CERN neutrino flux peaks at ~2 GeV, and the cut in $E_H \equiv \nu$ at 1 GeV increases the mean energy of the selected events somewhat. In the HPWF experiment, after a cut of $E_H > 4$ GeV the average energy of the antineutrino events is 41 GeV. With the same cut the average energy for the neutrino events varies from ~53 GeV to 85 GeV, depending on the beam used. Most of the CITF data comes from the lower peak of a dichromatic beam and has an average energy of 40 - 50 GeV after a cut $E_H > 12$ GeV.

In Fig. 1 we plot these ratios for the Weinberg-Salam model as functions of $\sin^2\theta_W$. In general one sees that for a given value of $\sin^2\theta_W$ $R^{\nu N} < R^{\nu p}$ while $R^{\bar{\nu}N} > R^{\bar{\nu}p}$. The solid curves represent the values below the threshold for charm production while the dashed curves represent the values calculated for energies far above charm threshold. The differences are easily understood; as the energy increases past the threshold for the production of c quarks and corresponding physical hadrons, the $\bar{s} \to \bar{c}$ transition increases $\sigma_{cc}^{\bar{\nu}}/E$. This transition occurs off sea quarks and hence is a rather small effect, but, (like the $\bar{d} \to \bar{u}$ contribution) it is not suppressed by a $(1 - y)^2$ dependence, as is the $u \to d$ transition. Since the neutral current in this model is diagonal in quark flavors it

yields a cross section which is not enhanced by new particle production. Consequently $R^{\bar{\nu}p}$ and $R^{\bar{\nu}N}$ decrease as one passes charm threshold. Similarly σ_{cc}^{ν}/E increases somewhat because of the $d \to c$ transition. Although this effect is of full valence strength it is suppressed by a factor $\sin^2 \theta_C$ and is not enhanced relative to the original transition $d \to u$ by a different y-dependence.

In connection with the discussion at the beginning of this section, it is of interest to see how rapidly the values of σ_{cc}^{ν}/E and $\sigma_{cc}^{\bar{\nu}}/E$ increase, or equivalently how rapidly R^{ν} and $R^{\bar{\nu}}$ decrease as functions of E. Taking a reasonable value for the Weinberg angle in this model, $\sin^2 \theta_W = 0.4$, a plausible mass for the c quark, $m_c = 1.5$ GeV, and finally a value $W_c \sim 3$ GeV for the corresponding physical threshold in invariant mass,[28] we calculate R^{ν} and $R^{\bar{\nu}}$ as functions of E. The resulting curves are shown in Fig. 2.

In Fig. 3 we plot the various neutral to charged current ratios for the six quark vector model. Since $\sigma_{nc}^{\nu} = \sigma_{nc}^{\bar{\nu}}$ in this model the dependence of $R^{\nu N}$ and $R^{\bar{\nu}N}$ on $\sin^2 \theta_W$ is the same, and hence one obtains straight lines. With appropriate changes the same statement holds for the ratios $R^{\nu p}$ and $R^{\bar{\nu}p}$. Again, the solid lines are the values below the c, b, and t quark thresholds while the dashed lines are the values far above these thresholds (so that $z_{c,\,b,\,t} \simeq x$). As in the Weinberg model, for a given value of $\sin^2 \theta_W$, $R^{\bar{\nu}N} > R^{\bar{\nu}p}$. In contrast to the former model, as $\sin^2 \theta_W$ increases from zero to one, both R^{ν} and $R^{\bar{\nu}}$

decrease, reach a minimum for $\sin^2 \theta_W \approx 0.8 - 0.9$ and then increase slightly.

As is evident from Fig. 4, the dependence of R^{ν} and $R^{\bar{\nu}}$ upon E is considerably more pronounced in the vector model than in the model of Weinberg and Salam. This is a consequence of the fact that the new particle production involves charged current transitions off valence, as well as sea, quarks which, moreover, are not suppressed by small angles. These are the transitions $d \to t$ in the neutrino case and $u \to b$ in the antineutrino case. The effect on $\sigma^{\bar{\nu}}$ is especially marked since asymptotically the (right-handed) $u \to b$ transition makes a contribution three times as great as the (left-handed) $u \to d$ transition. Fig. 4 shows how the decrease in these ratios occurs as the energy is increased. To obtain the curves of Fig. 4 we use[28] the effective quark masses, in units of GeV, $m_c = 1.5$, $m_b = 3.5$, and $m_t = 4.5$, and physical thresholds $W_c \simeq 3$, $W_b \simeq 5$, and $W_t = 6$. $R^{\bar{\nu}N}$ decreases by~30% from its value of 0.54 below charm threshold, to ~ 0.39 at $E \simeq 40$ GeV, which is the mean value of E for the HPWF measurement of this quantity. Over the same range of energy $R^{\nu N}$ decreases by $\sim 10\%$, from 0.24 to 0.22. From Fig. 3 one sees that for E far above flavor thresholds $R^{\nu N} = R^{\bar{\nu}N}$. It is clear why this is true since in this energy range $\sigma_{cc}^{\nu N} = \sigma_{cc}^{\bar{\nu}N}$ and for any energy $\sigma_{nc}^{\nu N} = \sigma_{nc}^{\bar{\nu}N}$.

Finally, the results for the Gürsey-Sikivie (B) and (C) models are shown in Figs. 5 - 6 and Figs. 7 - 8. The five-quark model of

Achiman et al. gives results which are quite similar to those of the G-S(B) model and are, accordingly, only shown in the summary plots (Figs. 9 and 10). From Figs. 5 and 7 one sees that R^{ν} and $R^{\bar{\nu}}$ for both isoscalar and proton targets decrease as $\sin^2 \theta_W$ increases from zero, reach minima for $\sin^2 \theta_W \simeq 0.7 - 0.8$ and then bend around and increase somewhat. For small $\sin^2 \theta_W$ the variation of the ratios is roughly linear.

The energy dependence of these ratios is depicted in Figs. 6 and 8 for $\sin^2 \theta_W = 0.4$. For this computation we have chosen[28] the following set of values for effective quark masses and physical thresholds, in units of GeV: $m_c = 1.5$, $m_b = m_{b'} = 4$, $W_c = 3$, $W_b = W_{b'} = 5.5$. Since $m_b = m_{b'}$ and $W_b = W_{b'}$ the cross sections are independent of the mixing angle ϕ. As in the vector model, from low energies of a few GeV to E = 40 GeV, $R^{\bar{\nu}N}$ drops considerably: by $\sim 30\%$ for G-S(B) model and by $\sim 40\%$ for the G-S(C) model. This is primarily a result of the excitation of the $u \to b$ and $u \to b'$ V + A transitions. In the G-S(C) model the neutral current is flavor-changing and consequently not only the charged current cross sections, but also the neutral current ones, increase with energy. However, the growth in $\left(\sigma_{nc}^{\nu,\ \bar{\nu}}/E\right)$ is small, since the flavor-changing transitions $d \to b$, $\bar{d} \to \bar{b}$, $s \to b'$, and $\bar{s} \to \bar{b}'$ are suppressed by the factor $\sin^2 \frac{\alpha}{2} \cos^2 \frac{\alpha}{2} \simeq 0.16$. (The latter three transitions would make small contributions to begin with because they involve sea quarks.)

In Fig. 9 we plot, on an expanded scale for each model considered, the ranges of $R^{\nu N}$ and $R^{\bar{\nu}N}$ which lie closest to the data. These curves

have been calculated for energies below the onset of heavy quark thresholds. The Weinberg-Salam model is in reasonably good agreement with the data, the optimal value of the Weinberg angle being given by $\sin^2 \theta_W \simeq 0.4$. The vector model predicts a line which lies somewhat below the data in $R^{\nu N}$ and above it in $R^{\bar{\nu}N}$. Indeed, the HPWF group states that its measurements of $\sigma_{cc}^{\bar{\nu}} / \sigma_{cc}^{\nu}$ and $R^{\bar{\nu}N}/R^{\nu N}$, give a value of $\sigma_{nc}^{\bar{\nu}N} / \sigma_{cc}^{\nu N}$ which lies ~ 3 standard deviations below the value of unity predicted by the vector model.[4] The CITF group asserts that its measurement[4] of these quantities implies a result for $\sigma_{nc}^{\bar{\nu}N} / \sigma_{nc}^{\nu N}$ which is 1.0 to 1.7 standard deviations away from a pure vector theory. The value $\sin^2 \theta_W \simeq 0.5$ yields the best agreement between the vector model results for $R^{\nu N}$ and $R^{\bar{\nu}N}$, and the inclusive data. In contrast, the G-S(B) and G-S(C) models agree reasonably well with the experimental measurements, the optimal value[29] of $\sin^2 \theta_W$ being ~ 0.4. Finally, Fig. 10 shows, again on an expanded scale, the predictions of the various models for $R^{\nu p}$ and $R^{\bar{\nu}p}$, as calculated below heavy quark thresholds.

IV. NEUTRINO-NUCLEON ELASTIC SCATTERING

The elastic and quasielastic scattering of neutrinos from nucleons has been the subject of a great deal of theoretical work over the past fifteen years.[30] We summarize here the basic expressions on which our computations are based.

The differential cross section is given in terms of six form factors: four first-class terms (g_V, f_V, g_A, and h_A), and two second-class terms (h_V and f_A). We omit the second-class terms since only first-class currents enter the gauge models of interest. Then the differential cross section takes the form

$$\frac{d\sigma}{dq^2}^{(\nu,\ \bar{\nu})} = \lambda \frac{G^2}{2\pi} \cdot \frac{1}{16\, M^2 E^2} \Big\{ (q^2 + m^2 - 4ME)^2 W_2 + (q^2 + m^2)\left[8M^2 W_1 - (q^2 + 4M^2)W_2 + m^2 W_4\right] \pm 2q^2(q^2 + m^2 - 4ME)W_3 \Big\} , \tag{4.1}$$

where E is the incident neutrino energy, M is the target nucleon mass, and m is the mass of the scattered lepton. The coupling strength is given by the Fermi constant, G, and the parameter[31]

$$\lambda = \begin{cases} \cos^2 \theta_C, & \text{quasielastic scattering} \\ 1, & \text{elastic scattering.} \end{cases} \tag{4.2}$$

The structure functions $W_1 \ldots W_4$ depend only upon $q^2 = -t \geq 0$.

For the quasielastic charged-current process $\nu n \to \mu^- p$ the structure functions are given by

$$\left.\begin{aligned} W_1 &= (1+\tau)G_A^2 + \tau G_M^2, \\ W_2 &= G_A^2 + (G_E^2 + \tau G_M^2)/(1+\tau), \\ W_3 &= -2G_M G_A, \\ W_4 &= -G_M^2 - G_A^2, \end{aligned}\right\} \qquad (4.3)$$

where CVC has been used to relate the weak and electromagnetic form factors, and $\tau \equiv q^2/4M^2$. The induced pseudoscalar term involving h_A has been dropped since it only enters proportional to m^2 and is difficult to measure. The form factors of the charged current are conventionally described by dipole forms as

$$\left.\begin{aligned} G_E(q^2) &= (1 + q^2/M_V^2)^{-2}, \\ G_M(q^2) &= 4.7(1 + q^2/M_V^2)^{-2}, \\ G_A(q^2) &= 1.24(1 + q^2/M_A^2)^{-2}, \end{aligned}\right\} \qquad (4.4)$$

with $M_V^2 = 0.71\ \text{GeV}^2$. The axial mass, M_A, is less precisely fixed. To illustrate the range of possibilities consistent with existing experimental

information, we present results for two values: $M_A^2 = 0.71$ and $1.32\ \text{GeV}^2$. An excellent review of two-body neutrino reactions has been given by Schreiner.[32]

For the elastic neutral current process, $\nu p \to \nu p$, we relate the structure functions $W_1 \ldots W_3$ (W_4 does not contribute) to the neutral current form factors G_E^0, G_M^0, and G_A^0 in analogy with Eq. (4.3). The neutral current form factors are taken to be proportional to the charged current form factors:

$$G_E^0(q^2) = \frac{1}{2}(\alpha + \gamma)G_E(q^2)$$

$$G_M^0(q^2) = \frac{1}{2}(\alpha + 0.88\ \gamma/4.7)G_M(q^2) \qquad (4.5)$$

$$G_A^0(q^2) = \frac{1}{2}(\beta + \delta)G_A(q^2) \quad .$$

The parameters α, β, γ, δ are specific to the models chosen for the neutral current interaction; they are listed in Table II for the models we consider. The isoscalar axial-vector part of the hadronic neutral current is negligible in the W-S model since it involves only strange and heavy quarks and consequently has small matrix elements between nucleon states. For the AKW and G-S(B) and (C) models the isoscalar axial vector current involves valence quarks and is not a priori negligible. One can estimate its contribution as follows. For definiteness, let us consider the G-S(B) model; with obvious changes the same method can be applied

to the AKW and G-S(C) models. With the neglect of strange and heavy quark currents, the ratio of the isoscalar to isovector form factors at $q^2 = 0$ is $\epsilon = 3 - 4\alpha_A$, where $\alpha_A = D/(D + F)$. Experimentally[33], $\alpha_A = 0.658 \pm 0.007$, and hence $\epsilon \simeq 0.368$. For lack of any experimental information, the q^2 dependence of the isoscalar axial vector form factor is assumed to be the same as its isovector analogue. Since the above estimate suffers from the lack of knowledge of this q^2 dependence of the isoscalar axial vector form factor, and since the changes in the cross sections (see below) are smaller than the uncertainty already present due to range of allowed values of M_A^2 and $\sin^2\theta_W$, we have judged it preferable to show only the results for $\epsilon = 0$.

We have computed the differential cross sections for elastic and quasielastic scattering in each of the models reviewed in Section II. To compare with the experimental results we have folded the theoretical distributions with a parametrization of the BNL neutrino spectrum,[34]

$$\frac{dN^{\nu}}{dE}(E) = \begin{cases} 0.12 \exp[-0.8(E-1.6)^2], & .5 < E < 2.4 \\ e^{-E} + .0133\, e^{-.3E}, & E > 2.4 \end{cases} \qquad (4.6)$$

where E is measured in GeV. This spectrum is not yet very well determined; however, as we shall discuss below, our results for neutrino scattering are relatively insensitive to its details.

In anticipation of measurements of $\bar{\nu}p$ elastic scattering, we have made predictions assuming the antineutrino spectrum also has the form (4.6). These are more dependent upon precise features of the spectrum, and may require some revision when the $\bar{\nu}$-spectrum has been determined in detail. Nevertheless, computations based upon the distribution (4.6) allow us to compare the expectations for neutrino and antineutrino scattering under conditions approximating the experimental ones.

To compare the predictions of the various models with data, we have imposed the appropriate experimental cuts. For the Harvard-Pennsylvania-Wisconsin experiment,[11] the restriction is a simple q^2-cut: $0.3 \leq q^2 \leq 0.9$ GeV^2. For the Columbia-Illinois-Rockefeller experiment,[11] the recoil proton is required to have a laboratory momentum greater than 550 MeV/c and a recoil angle in the laboratory greater than 25°. We have ignored effects due to nuclear targets. Yao's analysis[35] shows that they are quite small for $q^2 > 0.3$ GeV^2.

The predicted values of

$$R_{el}^{\nu} \equiv \sigma(\nu p \to \nu p)/\sigma(\nu n \to \mu^- p) \tag{4.7}$$

and

$$R_{el}^{\bar{\nu}} \equiv \sigma(\bar{\nu}p \to \bar{\nu}p)/\sigma(\bar{\nu}p \to \mu^+ n)$$

as functions of the Weinberg angle are compared with the experimental results in Figs. 11 - 14. The theoretical curves plotted are those appropriate for the HPW cuts. Those for the CIR cuts have been omitted for clarity; they differ only slightly from the HPW predictions, as we shall discuss below. The full curves are computed with $M_A^2 = 0.71\ \text{GeV}^2$; the dashed curves correspond to $M_A^2 = 1.32\ \text{GeV}^2$. In each figure, the shaded bands represent the HPW values

$$R_{el}^{\nu} = 0.17 \pm 0.05$$
$$R_{el}^{\bar{\nu}} = 0.2 \pm 0.1.$$

The CIR value,

$$R_{el}^{\nu} = 0.23 \pm 0.09$$

is denoted by a point at our favored value of $\sin^2 \theta_W$.

The prediction of the Weinberg-Salam model lies approximately 1.5 standard deviations below the νp data, but agrees well with the $\bar{\nu}p$ value. That of the vector model lies at least two standard deviations below the νp data, but is in reasonable agreement with the $\bar{\nu}p$ value. The Gürsey-Sikivie models (B) and (C) (with $\epsilon = 0$)[33] are both in agreement with the νp and $\bar{\nu}p$ data. As an example of the effect of including the isoscalar axial vector current, in the (B) model R_{el}^{ν} decreases by ~10% for $M_A^2 = 0.71\ \text{GeV}^2$ and by ~15% for $M_A^2 = 1.32\ \text{GeV}^2$, while $R_{el}^{\bar{\nu}}$ is essentially unchanged for $M_A^2 = .71\ \text{GeV}^2$ and decreases by ~4% for $M_A^2 = 1.32\ \text{GeV}^2$. The five-quark model of Achiman, Koller, and Walsh interpolates between the Weinberg-Salam model and the Gürsey-Sikivie model (B) as $\cos \phi$ ranges between 0 and 1. In all models considered, the ratio $R_{el}^{\bar{\nu}}$ is expected to be significantly larger than R_{el}^{ν}.

Let us briefly take up the questions of energy-dependence and experimental cuts. We show in Table IV the predictions of the four models for incident energies of 1.5 GeV and 10 GeV, for the HPW and CIR cuts and no cuts. In all the models, R_{el}^{ν} increases slightly with neutrino energy, while $R_{el}^{\bar{\nu}}$ decreases more markedly. This behavior can be understood from the energy dependences of the quasielastic and elastic cross sections shown in Fig. 15. The quasielastic antineutrino reaction cross section doubles above 1 GeV, whereas the quasielastic neutrino reaction cross section decreases slightly. The cross sections for both the elastic reactions (here computed for the Weinberg-Salam model with $\sin^2\theta_W = 0.4$) increase by about 15 % between 1 and 10 GeV. The entries in Table IV also justify our earlier claim that the two kinds of experimental cuts lead to essentially identical theoretical expectations.

We now turn to the differential cross sections. We plot in Figs. 16 - 19 the predictions of the four models for the reactions $\nu n \to \mu^- p$ and $\nu p \to \nu p$, folded with the BNL neutrino spectrum (4.6), for our two choices of the axial vector mass. The theoretical curves are given with absolute normalization. The full curves are for $M_A^2 = 0.71$; the dashed curves correspond to $M_A^2 = 1.32$. The HPW data[11] are plotted as events. We have assumed agreement between theory and experiment for the quasielastic cross section, and we test the predictions of the models for elastic scattering.

The Weinberg-Salam model gives a good description of the shape of the differential cross section, but (as we noted in connection with Fig. 11) yields a smaller cross section than is observed. The vector

model prediction is significantly flatter than the data.[36] Both versions (B) and (C) of the Gürsey-Sikivie model are in excellent agreement with the published data.

It is possible for the reaction

$$\nu n \to \nu n \tag{4.8}$$

to mimic νp elastic scattering by virtue of np charge exchange within the detector. Whether this effect is important can only be judged by the experimenters themselves.[37] We wish to note, however, that theoretically the νn elastic cross section is quite comparable with $\sigma_{el}(\nu p)$. We show in Fig. 20 our prediction for the $\nu n \to \nu n$ differential cross section at BNL, in the Weinberg-Salam model. Roughly speaking, $d\sigma(\nu n)/dq^2 \approx 1.5\, d\sigma(\nu p)/dq^2$ over the range $0 \leq q^2 \leq 1\ \text{GeV}^2$. Similarly, we find that $d\sigma(\bar{\nu}n)/dq^2 \approx d\sigma(\bar{\nu}p)dq^2$. In the vector model, the cross section for scattering off neutrons is about 1/3 that for scattering off protons. In model (B) of Gürsey and Sikivie, $d\sigma(\nu n)/dq^2 \approx 1/3\, d\sigma(\nu p)/dq^2$ and $d\sigma(\bar{\nu}n)/dq^2 \approx 1/4\, d\sigma(\bar{\nu}p)/dq^2$. If some of the reported νp elastic scattering events were to be attributed to νn contamination, agreement between the Weinberg-Salam model and experiment would be improved.

We show in Figs. 21-24 the predictions for the differential cross sections $d\sigma/dq^2(\bar{\nu}p \to \mu^+ n)$ and $d\sigma/dq^2(\bar{\nu}p \to \bar{\nu}p)$, folded with the BNL spectrum (4.6). All models, with the possible exception of the vector model, are in agreement with the $\bar{\nu}p \to \bar{\nu}p$ data. Fig. 25 illustrates the dependence

of the ratio of flux-averaged cross sections, $\sigma(\bar{\nu}p \to \bar{\nu}p)/\sigma(\nu p \to \nu p)$, on $\sin^2\theta_W$. We emphasize that any calculation of this ratio is sensitively dependent upon the form taken for the neutrino and antineutrino flux spectra. It might be noted that in the Weinberg-Salam model, for $\sin^2\theta_W = 0.4$ this ratio is ~ 0.9 and consequently it would be difficult to detect parity violation by observation of differences between νp and $\bar{\nu}p$ elastic scattering. However, if one were to use the value $\sin^2\theta_W = 0.3$, which is also consistent with the deep inelastic inclusive data, the ratio decreases to ~ 0.6. Establishing parity violation will of course also be complicated by any differences between the spectra of incident neutrinos and antineutrinos.

V. CONCLUSIONS

Experiments on neutral current interactions have moved from the discovery phase to detailed investigation of the structure of the neutral current. It is now possible to require that models for the weak interactions account for many different neutral current observables at once.

In the deep-inelastic regime, forthcoming measurements of the ratios $R^{\nu p}$ and $R^{\bar{\nu}p}$ of the neutral current cross section to charged current cross section will impose important additional constraints on models of the weak current.

Given measurements of $R^{\nu N}$ and $R^{\bar{\nu}N}$ below new flavor thresholds,[5] we find that the two experiments,[11] on νp elastic scattering provide nontrivial tests of models, which can be augmented by measurements of $\bar{\nu}p$ elastic scattering. Having constrained the Weinberg angle in all

models by requiring optimal agreement with deep inelastic data on $R^{\nu N}$ and $R^{\bar{\nu}N}$, we have confronted these models with the elastic scattering data and arrived at the following judgments.

The Weinberg-Salam model[2] satisfactorily describes the slope of the differential cross section for νp and $\bar{\nu}p$ elastic scattering. It also is in agreement with the integrated $\bar{\nu}p$ cross section but predicts a value of $\sigma^{\bar{\nu}p}$ which is too small by about 1.5 standard deviations. In view of the possible presence in the data of contamination from the reaction $\nu n \to \nu n$, this model still must be regarded as an entirely adequate description of elastic scattering. However, it is not rich enough to describe satisfactorily all the phenomena observed in deep-inelastic scattering at high energies.

The vector models[15] are in significant disagreement with the differential cross section for νp elastic scattering. These models are also in serious conflict with high-energy data on deep-inelastic scattering.

The Gürsey-Sikivie models (B) and (C)[17] are in excellent agreement with the νp and $\bar{\nu}p$ elastic scattering data in magnitude and shape. Both models (B) and (C) also appear to agree with the trends of the deep-inelastic scattering data at high energies.

We may now look forward to further tests of weak interaction models by improved data on νp elastic scattering, by further measurements of $\bar{\nu}p$ elastic scattering, and ideally by separation of $(\nu, \bar{\nu})n$ elastic scattering events. This promises to be a topic for fruitful interaction between theory and experiment.

ACKNOWLEDGMENTS

We thank D. P. Sidhu for communicating the results of his evaluation of R_{el} in the Weinberg model.[38] We have also enjoyed conversations with E. Fischbach and S. P. Rosen regarding their work on SPT models. We are grateful to W. Lee, A. K. Mann, L. Sulak, and H. H. Williams for discussions of their experiments. We thank S. B. Treiman for a valuable suggestion and R. M. Barnett for comments. Finally, we thank B. W. Lee for his continuing interest in this work.

Note added: While preparing this manuscript for publication, we received a related preprint from Barger and Nanopoulos.[39] The corrected version of their article is in agreement with our results, where the two works overlap.

FOOTNOTES AND REFERENCES

[1]F. J. Hasert et al., Phys. Lett. 46B,121, 138 (1973), Nucl. Phys. B73, 1 (1974); A. Benvenuti et al., Phys. Rev. Lett. 32, 800 (1974); B. Aubert et al., ibid. 32, 1454, 1457 (1974); S. J. Barish et al., ibid. 33, 468 (1974); B. C. Barish et al., ibid. 34, 538 (1975). See also the following talks in Proc. XVI International Conference on High Energy Physics, ed. J. R. Smith (Chilton: Rutherford Laboratory, 1974); B. C. Barish, p. IV-111, A. Pullia, p. IV-114, C. Rubbia, p. IV-117, J. Sacton, p. IV-121, P. Schreiner, p. IV-123, W. Lee, p. IV-127, A. Rousset, p. IV-128, and D. C. Cundy, p. IV-131.

[2]S. L. Glashow, Nucl. Phys. 22, 579 (1961); A. Salam and J. Ward, Phys. Lett. 13, 168 (1964); S. Weinberg, Phys. Rev. Lett. 19, 1264 (1967), ibid. 27, 1688 (1971). A. Salam, in Elementary Particle Theory, ed. N. Svartholm (Stockholm: Almquist and Wiksell, 1969), p. 367.

[3]See the review talks by D. C. Cundy, Ref. 2; H. Faissner, invited talk at the 1975 Neutrino Conference, Balatonfüred, Aachen preprint PITHA-(1975)84; J. G. Morfin, in Proc. 1975 International Symposium on Lepton and Photon Interactions at High Energies, ed. W. T. Kirk (Stanford: SLAC, 1976), p. 537; D. H. Perkins, ibid., p. 571.

[4]J. G. Morfin and D. H. Perkins, Ref. 3, V. Brisson, talk given at the Rencontre de Moriond, Flaine (1976), and D. C. Cundy, private communication; L. Stutte, talk given at the Conference on the Production

of Particles with New Quantum Numbers, Madison, (1976); A. Benvenuti et al., HPWF preprint No. 76/4.

[5]For the HPWF data, see D. Cline, talks given at the Palermo Conference (June, 1975) and the Irvine Conference (December, 1975); C. Rubbia in the Proceedings of the 1975 International Symposium on Lepton and Photon Interactions at High Energies, Stanford, op. cit., p. 1049, A. K. Mann, talk given at "Orbis Scientiae," Coral Gables (January, 1976), A. Benvenuti et al., HPWF preprint Nos. 76/1, 76/2, 76/3, and 76/4. For the CITF data see B. C. Barish, in the Proceedings of the 1975 International Symposium on Lepton and Photon Interaction at High Energies, Stanford, op. cit., p. 511, F. Sciulli, in Particles and Fields 1975, eds., H. Lubatti and P. Mockett (Seattle, University of Washington Press, 1976), p. 76, and L. Stutte, Ref. 4. For the Fermilab 15' bubble chamber data, see J. P. Berge et al., Phys. Rev. Lett. 36, 639 (1976), M. Derrick et al., Phys. Rev. Lett. 36, 936 (1976), and W. Scott, talk given at the Vanderbilt Conference (April, 1976).

[6]F. A. Harris et al., Fermilab-Hawaii-LBL-Michigan collaboration, Bull. Am. Phys. Soc., 21, 16 (1976), abstract AG-5; V. Z. Peterson et al., ibid., 546, abstract BL-6; A. T. Laasanen et al., Purdue-Argonne-Carnegie-Mellon collaboration, ibid., 547, abstract BL-12; M. Derrick and F. Nezrick, private communication.

[7]L. G. Hyman, in La Physique du neutrino à Haute Energie, (Paris: CNRS, 1975), p. 183; W. Lee, ibid., p. 205; J. P. Vialle, ibid., p. 225.

[8]B. Coremans et al., Phys. Lett. 61B, 207 (1976); W. Y. Lee, private communication; M. Derrick, remarks at the Conference on the Production of Particles with New Quantum Numbers, Madison.

[9]N. Samios, in the Proceedings of the 1975 Stanford Symposium, op. cit., p. 527;J. von Krogh et al., Phys. Rev. Lett. 36, 710 (1976); J. Blietschau et al., Phys. Lett. 60B, 207 (1976).

[10]See the papers of Ref. 9 and: B. Roe, in the Proceedings of the 1975 Stanford Symposium, op. cit., p. 551; J. P. Berge et al., Phys. Rev. Lett. 36, 127 (1976); M. Derrick, in Ref. 5; M. Murtagh, talk delivered at the Madison Conference.

[11]W. Lee, E. Maddry, W. Sippach, P. Sokolsky, L. Teig, A. Bross, T. Chapin, L. Nodulman, T. O'Halloran, C. Y. Pang, K. Goulianos, and L. Litt, Phys. Rev. Lett. (to be published), and W. Lee, private communication; D. Cline, A. Entenberg, W. Kozanecki, A. K. Mann, D. D. Reeder, C. Rubbia, J. Strait, L. Sulak, and H. H. Williams, Phys. Rev. Lett. (to be published), and L. Sulak, private communication.

[12]Evidence on $\nu_\mu e$ and $\bar{\nu}_\mu e$ scattering is discussed by F. J. Hasert, et al. Phys. Lett. 46B, 121 (1973); J. G. Morfin, Ref. 3; H. Faissner, invited talk at the EPS International Conference on High Energy Physics at

Palermo, 1975, Aachen preprint PITHA-(1975)85. The most recent published results of the Irvine-Savannah River reactor experiment on $\bar{\nu}_e e$ scattering are contained in F. Reines. H. W. Sobel, and H. S. Gurr, Irvine preprint UCI-10P-19-90.

[13] B. Kayser, G. T. Garvey, E. Fischbach, and S. P. Rosen, Phys. Lett. 52B, 385 (1975); R. L. Kingsley, R. Shrock, S. B. Treiman, and F. Wilczek, Phys. Rev. D11, 1043 (1975) and references therein; S. Adler et al., Phys. Rev. D11, 3309, D12, 3501 (1975); S. Adler, Hawaii Summer School Lectures (1975); J. J. Sakurai, CERN preprint TH. 2099. The Fermilab inclusive neutrino data on y distributions (see, e.g. F. Sciulli, Ref. 5) rule out a pure (S, P) hadronic neutral current, which would predict that $d\sigma^{\nu}/dy$ and $d\sigma^{\bar{\nu}}/dy$ are proportional to y^2.

[14] J. T. Gruenwald, E. Fischbach, S. P. Rosen, H. Spivack, and B. Kayser, Bull. Am. Phys. Soc. 21, 17 (1976), abstract AG10; E. Fischbach, et al., to be published.

[15] F. Wilczek, A. Zee, R. Kingsley, and S. B. Treiman, Phys. Rev. D12, 2768 (1975); H. Fritzsch, M. Gell-Mann, and P. Minkowski, Phys. Lett. 59B, 256 (1975); A. De Rújula, H. Georgi, and S. L. Glashow, Phys. Rev. D12, 3589 (1975); S. Pakvasa, L. Pilachowski, W. A. Simmons and S. F. Tuan, Hawaii preprint (December, 1975).

[16] Y. Achiman, K. Koller, and T. F. Walsh, Phys. Lett. 59B, 261 (1975). This model has also been discussed by B. W. Lee at the Washington A. P. S. meeting (April, 1976).

[17] P. Fayet, Nucl. Phys. B78, 14 (1974);
F. Gürsey and P. Sikivie, Phys. Rev. Lett. 36, 775 (1976); P. Ramond, Caltech preprint CALT-68-540, to be published; R. M. Barnett, Phys. Rev. Lett. 34, 41 (1975); Phys. Rev. D11, 3246 (1975).

[18] It should be noted that there exist theories which embed the weak gauge group and the color SU(3) gauge group in an overall simple group. In such theories, mixing angles such as θ_W are not arbitrary parameters but rather are determined by the structure of the embedding of the various subgroups in the full group. The Gürsey-Sikivie theory is one such example.

[19] Many of the gauge models incorporate heavy leptons in the left-handed and right-handed multiplets, but these are not important for the ordinary charged and neutral current reactions we consider here.

[20] S. L. Glashow, J. Iliopoulos and L. Maiani, Phys. Rev. D2, 1285 (1970).

[21] The vector models originally proposed by A. De Rújula, H. Georgi, and S. L. Glashow (Phys. Rev. Lett. 35, 702 (1975)) and S. Pakvasa, W. Simmons, and S. F. Tuan (Phys. Rev. Lett 35, 702 (1975)) contained a $\binom{c}{d}_R$ doublet. It was shown in Refs. 22 and 23 that this conflicts with experiment. Accordingly, the models of De Rújula et al. and Pakvasa et al. in Ref. 15 avoided the $\binom{c}{d}_R$ doublet.

[22] E. Golowich and B. R. Holstein, Phys. Rev. Lett. 35, 831 (1975).

[23] F. Wilczek, A. Zee, R. Kingsley, and S. B. Treiman in Ref. 15. See also G. Branco, T. Hagiwara, and R. N. Mohapatra, Phys. Rev. D13, 104 (1976).

[24] L. Stutte and A. Benvenuti et al., in Ref. 5.

[25] F. Gürsey and S. Orfandis, Nuovo Cimento 11A, 225 (1972); O. W. Greenberg and D. Bhaumik, Phys. Rev. D4, 2048 (1971); G. Domokos, Phys. Rev. D4, 3708 (1971); O. Nachtmann, Nucl. Phys. B63, 237 (1973); and H. Georgi and H. D. Politzer, Phys. Rev. Lett. 36, 1281 (1976) and Harvard preprint.

[26] S. Pakvasa, D. Parashar, and S. F. Tuan, Phys. Rev. D10, 2124 (1974); see also J. Okada, S. Pakvasa, and S. F. Tuan, Hawaii preprint UH-511-209-76.

[27] R. D. Field, private communication.

[28] C. H. Albright and R. E. Shrock, to be published. Similar calculations have been done by S. Pakvasa, L. Pilachowski, W. A. Simmons, and S. F. Tuan, Ref. 15; R. M. Barnett, Phys. Rev. Lett. 36, 1163 (1976), Harvard preprint (February, 1976); and V. Barger, T. Weiler, and R. Philips, Wisconsin preprint (April, 1976).

[29] In the Gürsey-Sikivie E_7 models, the angle θ_W is not a free parameter. The unrenormalized value of $\sin^2 \theta_W$ is 0.75, but renormalization effects due to the presence of superheavy vector bosons are expected to reduce this value to $\sim$0.50. It appears difficult to reduce this as low as 0.40 (see Ref. 17). However, from a phenomenological point of view it is still of interest to test the predictions which follow from the structure of quark multiplets in these models, independently of the general unification scheme with its resulting constraint on θ_W.

[30]On the quasi-elastic reactions, see T. D. Lee and C. N. Yang, Phys. Rev. Lett. 4, 307 (1960), ibid., Phys. Rev. 126, 2239 (1962); N. Cabibbo and R. Gatto, Nuovo Cimento 15, 304 (1960); Y. Yamaguchi, Prog. Theor. Phys. 23, 1117 (1960); S. L. Adler, Phys. Rev. 135, B963 (1964); Y. P. Yao, Phys. Rev. 176, 1680 (1968); A. Pais, Ann. Phys. (N.Y.) 63, 361 (1971). On the elastic reactions, see S. Weinberg, Phys. Rev. D5, 1412 (1972), J. J. Sakurai and L. F. Urrutia, Phys. Rev. D11, 159 (1975), and F. Martin, Nucl. Phys. B104, 111 (1976).

[31]As was discussed in section II, if one generalizes the Higgs representation content the neutral current cross sections are scaled relative to the charged current ones by the factor κ^2, where κ is defined in Eq. (2.4). The deep inelastic data on $R^{\nu N}$ and $R^{\bar{\nu}N}$ indicate that κ cannot be very different from unity in Weinberg-Salam model. This is because in the region near the data (see Fig. 9) a variation in $\sin^2\theta$ causes the ($R^{\nu N}$, $R^{\bar{\nu}N}$) point to move in a direction roughly orthogonal to a straight line emanating from the origin, which is the trajectory along which the point travels as κ is scaled up or down from unity. In contrast, in this region the trajectories followed by the point ($R^{\nu N}$, $R^{\bar{\nu}N}$) in the vector, five-quark, G-S(B), and G-S(C) models as $\sin^2\theta_W$ is varied are roughly parallel to lines emanating from the origin. Hence in these latter models a change in $\sin^2\theta_W$ can be cancelled by an appropriately chosen change in κ and we cannot conclude that κ must be near one.

[32]P. A. Schreiner, in Neutrino 1974, ed. C. Baltay (New York: American Institute of Physics, 1974), p. 101.

[33] K. Kleinknecht, in Proceedings of the XVI International Conference on High Energy Physics, op cit., p. III-23. We thank S. B. Treiman for a discussion on the isoscalar axial vector form factor. Note that the resulting value of ϵ, viz. $\epsilon \simeq 0.37$, is somewhat smaller than the SU(6) prediction, $\epsilon = 0.6$. For a calculation based on the assumption of SU(6) symmetry rather than the experimental value of α_A, see R. M. Barnett, Harvard preprint (June 1976).

[34] This is a preliminary version of the BNL neutrino spectrum based on the Sanford-Wang π, K spectra (see BNL Report 11299, parts 1 and 2 (1967)). We thank M. Murtagh for discussions on the BNL neutrino spectrum.

[35] Y. P. Yao, in Ref. 30.

[36] We have based our determination of $\sin^2 \theta_W$ in the vector model (as in the others) on an analysis of the inclusive data since they have by far the greatest statistical weight. We should remark that the exact value $\sin^2 \theta_W = 0.5$ would actually lead to a vanishing rate for the reactions $\nu_\mu e \to \nu_\mu e$ and $\bar{\nu}_\mu e \to \bar{\nu}_\mu e$. Although 3 ± 1.8 $\bar{\nu}_\mu e \to \bar{\nu}_\mu e$ events have been observed[12] the above value of $\sin^2 \theta_W$ is allowed at the 90% confidence level by this data. Moreover, our selection of an optimal Weinberg angle for the inclusive data is obviously approximate; if we were to take $\sin^2 \theta_W = 0.55$, for example, which again is consistent with the leptonic data, none of our conclusions would be changed. It should also be noted that our value of $\sin^2 \theta_W$ differs from the value of 0.68 selected by

De Rújula, Georgi, and Glashow (DGG) for their vector-like theory, Ref. 21. Both numbers are based on a comparison of the theoretical predictions for $R^{\nu N}$ and $R^{\bar{\nu}N}$, as calculated below heavy quark thresholds, with the data. Hence the fact that the DGG model differs in the structure of the right-handed quark doublets from the vector model (of Ref. 15) has no effect; both models yield the same neutral current cross sections and, below heavy quark thresholds, also the same charged current cross sections. The reason for the difference in the optimal value of $\sin^2 \theta_W$ is that DGG based their determination upon the HPWF measurements of $R^{(\nu, \bar{\nu})N}$ then available, which were: $R^{\nu N} = 0.11 \pm 0.05$, $R^{\bar{\nu}N} = 0.32 \pm 0.09$. (B. Aubert et al., Phys. Rev. Lett. 32, 1454, 1457 (1974)). However, on the basis of a later, enlarged data sample the HPWF group obtained the values listed in Table III, which we have used for our study.

[37] We thank W. Lee, A. K. Mann and L. Sulak for discussions on the problem of the background due to the reaction $\nu n \to \nu n$ followed by charge exchange.

[38] D. P. Sidhu, Brookhaven Report, in preparation.

[39] V. Barger and D. V. Nanopoulos, Wisconsin preprint.

Table I. Left-handed and right-handed doublet structure for the SU(2)⊗U(1) models considered in the text.

Model	Left-handed Doublets	Right-handed Doublets
Weinberg-Salam	$\begin{pmatrix} u \\ d_\theta \end{pmatrix}_L, \begin{pmatrix} c \\ s_\theta \end{pmatrix}_L$	-------
Vector	$\begin{pmatrix} u \\ d_\theta \end{pmatrix}_L, \begin{pmatrix} c \\ s_\theta \end{pmatrix}_L, \begin{pmatrix} t \\ b \end{pmatrix}_L$	$\begin{pmatrix} u \\ b \end{pmatrix}_R, \begin{pmatrix} c \\ s \end{pmatrix}_R, \begin{pmatrix} t \\ d \end{pmatrix}_R$
Achiman, Koller, Walsh	$\begin{pmatrix} u \\ d_\theta \end{pmatrix}_L, \begin{pmatrix} c \\ s_\theta \end{pmatrix}_L$	$\begin{pmatrix} u_\phi \\ b \end{pmatrix}_R$
Gürsey-Sikivie (B)	$\begin{pmatrix} u \\ d_\theta \end{pmatrix}_L, \begin{pmatrix} c \\ s_\theta \end{pmatrix}_L$	$\begin{pmatrix} u \\ b_\phi \end{pmatrix}_R, \begin{pmatrix} c \\ s \end{pmatrix}_R$
Gürsey-Sikivie (C)	$\begin{pmatrix} u_\alpha \\ d_\alpha \end{pmatrix}_L, \begin{pmatrix} c_\alpha \\ b'_\alpha \end{pmatrix}_L$	$\begin{pmatrix} u \\ b_\phi \end{pmatrix}_R, \begin{pmatrix} c \\ s \end{pmatrix}_R$

Table II. Isovector and isoscalar parameters for the neutral currents in the five models of interest.[a]

Model	α	β	γ	δ
W-S	$1 - 2\sin^2\theta_W$	1	$-2\sin^2\theta_W$	0
Vector	$2 - 2\sin^2\theta_W$	0	$-2\sin^2\theta_W$	0
AKW	$1 + \frac{1}{2}\cos^2\phi - 2\sin^2\theta_W$	$1 - \frac{1}{2}\cos^2\phi$	$\frac{3}{2}\cos^2\phi - 2\sin^2\theta_W$	$-\frac{1}{2}\epsilon\cos^2\phi$
G-S (B)	$\frac{3}{2} - 2\sin^2\theta_W$	$\frac{1}{2}$	$\frac{3}{2} - 2\sin^2\theta_W$	$-\frac{1}{2}\epsilon$
G-S (C)	$1 + \frac{1}{2}\cos^2\frac{\alpha}{2} - 2\sin^2\theta_W$	$\frac{1}{2}\cos^2\frac{\alpha}{2}$	$3 - \frac{3}{2}\cos^2\frac{\alpha}{2} - 2\sin^2\theta_W$	$-\frac{1}{2}\epsilon\cos^2\frac{\alpha}{2}$

[a] The parameter ϵ represents the relative ratio of the isoscalar to isovector axial current matrix elements.

Table III. Experimental values of $R^{\nu N}$ and $R^{\bar{\nu}N}$ for the CERN Gargamelle, Harvard-Pennsylvania-Wisconsin-Fermilab, and Caltech-Fermilab experimental collaboration.

Experiment	$R^{\nu N}$	$R^{\bar{\nu}N}$
CERN GGM	0.22 ± 0.03[a]	0.43 ± 0.12[a]
	0.28 ± 0.04[b]	0.38 ± 0.06[b]
HPWF	0.29 ± 0.04[c]	0.39 ± 0.10[c]
CITF	0.24 ± 0.04[d]	0.35 ± 0.11[d]

(a) F. H. Hasert et al., Nucl. Phys. B73, 1 (1974); D. C. Cundy, Ref. 1. (The first reference quotes an error of $\pm$ 0.04 on R^{ν}; the second and later one gives $\pm$ 0.03, which we have accordingly used.) J. Morfin, Ref. 3.

(b) V. Brisson, talk given at the Rencontre de Moriond, Flaine (1976); D. C. Cundy, private communication.

(c) A. Benvenuti et al., HPWF preprint No. 76/4. This supersedes the earlier results $R^{\nu} = 0.11 \pm 0.05$ and $R^{\bar{\nu}} = 0.32 \pm 0.09$ given by B. Aubert, et al., Phys. Rev. Lett. 32, 1454, 1457 (1974).

(d) L. Stutte, talk given at the Conference on the Production of Particles with New Quantum Numbers, Madison (April, 1976).

Table IV. Energy Dependence of the Ratios R_{el}^{ν} and $R_{el}^{\bar{\nu}}$.

Model	Energy, GeV	Cuts	R_{el}^{ν}		$R_{el}^{\bar{\nu}}$	
			$M_A^2 = 0.71$	$M_A^2 = 1.32$	$M_A^2 = 0.71$	$M_A^2 = 1.32$
W-S	1.5	none	0.099	0.118	0.174	0.242
$\sin^2\theta_W = 0.4$	10		0.114	0.144	0.125	0.164
	1.5	HPW	0.071	0.103	0.157	0.262
	10		0.090	0.135	0.100	0.154
	1.5	CIR	0.065	0.097	0.154	0.297
	10		0.084	0.131	0.095	0.156
Vector,	1.5	none	0.052	0.039	0.097	0.084
$\sin^2\theta_W = 0.5$	10		0.068	0.051	0.076	0.059
	1.5	HPW	0.067	0.046	0.166	0.128
	10		0.088	0.062	0.100	0.072
	1.5	CIR	0.070	0.046	0.192	0.155
	10		0.092	0.063	0.107	0.076
G-S (B)	1.5	none	0.188	0.161	0.255	0.220
$\sin^2\theta_W = 0.4$	10		0.209	0.175	0.220	0.185
$\epsilon = 0$	1.5	HPW	0.172	0.144	0.263	0.204
	10		0.200	0.162	0.211	0.169
	1.5	CIR	0.167	0.139	0.267	0.206
	10		0.196	0.157	0.210	0.167
G-S (C)	1.5	none	0.196	0.160	0.293	0.250
$\sin^2\theta_W = 0.4$	10		0.226	0.181	0.241	0.196
$\epsilon = 0$	1.5	HPW	0.168	0.134	0.293	0.223
	10		0.207	0.160	0.223	0.172
	1.5	CIR	0.160	0.126	0.295	0.226
	10		0.201	0.152	0.219	0.167

FIGURE CAPTIONS

Fig. 1: The ratios $R^{(\nu,\ \bar{\nu})N}$ and $R^{(\nu,\ \bar{\nu})p}$ as functions of $\sin^2\theta_W$ in the Weinberg-Salam model. The solid curves are (a) $(R^{\nu N},\ R^{\bar{\nu}N})$ and (b) $(R^{\nu p},\ R^{\bar{\nu}p})$ for E below charm threshold. The dashed curves are (c) $(R^{\nu N},\ R^{\bar{\nu}N})$ and (d) $(R^{\nu p},\ R^{\bar{\nu}p})$ for E far above charm threshold. The variation of $\sin^2\theta_W$ from 0 to 1 along each curve is indicated by tick marks at each tenth of a unit.

Fig. 2: The ratios $R^{(\nu,\ \bar{\nu})N}$ and $R^{(\nu,\ \bar{\nu})p}$ as functions of E in the Weinberg-Salam model with $\sin^2\theta_W = 0.4$.

Fig. 3: The ratios $R^{(\nu,\ \bar{\nu})N}$ and $R^{(\nu,\ \bar{\nu})p}$ as functions of $\sin^2\theta_W$ in the vector model. The solid lines are (a) $(R^{\nu N},\ R^{\bar{\nu}N})$ and (b) $(R^{\nu p},\ R^{\bar{\nu}p})$ for E below heavy quark thresholds. The dashed lines are (c) $(R^{\nu N},\ R^{\bar{\nu}N})$ and (d) $(R^{\nu p},\ R^{\bar{\nu}p})$ for E far above these thresholds. The variation of $\sin^2\theta_W$ from 0 to 1 along each line is indicated by tick marks at each tenth of a unit.

Fig. 4: The ratios $R^{(\nu,\ \bar{\nu})N}$ and $R^{(\nu,\ \bar{\nu})p}$ as functions of E in the vector model with $\sin^2\theta_W = 0.5$.

Fig. 5: The ratios $R^{(\nu,\ \bar{\nu})N}$ and $R^{(\nu,\ \bar{\nu})p}$ as functions of $\sin^2\theta_W$ in the Gürsey-Sikivie model (B). The solid curves are (a) $(R^{\nu N},\ R^{\bar{\nu}N})$ and (b) $(R^{\nu p},\ R^{\bar{\nu}p})$ for E below heavy quark thresholds. The dashed curves are (c) $(R^{\nu N},\ R^{\bar{\nu}N})$ and

(d) ($R^{\nu p}$, $R^{\bar{\nu}p}$) for E far above these thresholds. The variation of $\sin^2\theta_W$ from 0 to 1 along the curves is indicated by tick marks at each tenth of a unit.

Fig. 6: The ratios $R^{(\nu,\ \bar{\nu})N}$ and $R^{(\nu,\ \bar{\nu})p}$ as functions of E in the Gürsey-Sikivie model (B) with $\sin^2\theta_W = 0.4$.

Fig. 7: The ratios $R^{(\nu,\ \bar{\nu})N}$ and $R^{(\nu,\ \bar{\nu})p}$ as functions of $\sin^2\theta_W$, as in Fig. 5, but for the Gürsey-Sikivie model (C).

Fig. 8: The ratios $R^{(\nu,\ \bar{\nu})N}$ and $R^{(\nu,\ \bar{\nu})p}$ as functions of E in the Gürsey-Sikivie model (C) with $\sin^2\theta_W = 0.4$.

Fig. 9: The ratios $R^{\nu N}$ and $R^{\bar{\nu}N}$ as functions of $\sin^2\theta_W$ for the Weinberg-Salam (W-S), vector, Gürsey-Sikivie (G-S) models (B) and (C), and the five-quark model of Achiman et al. The curves are calculated for E below heavy quark thresholds. The tick marks on each curve denote the value of $\sin^2\theta_W$. See Table III for a list of the data points and relevant references.

Fig. 10: The ratios $R^{\nu p}$ and $R^{\bar{\nu}p}$ as functions of $\sin^2\theta_W$ for the Weinberg-Salam(W-S), vector, Gürsey-Sikivie (G-S) models (B) and (C), and the five-quark model. The curves are calculated for E below heavy quark thresholds.

Fig. 11: (a) Ratio $R_{el}^{\ \nu}$ of elastic to quasielastic neutrino-proton cross sections in the Weinberg-Salam model. Theoretical curves are for the experimental conditions of the HPW

measurement. The solid curve corresponds to an axial form factor with $M_A^2 = 0.71\ GeV^2$; the dashed curve is for $M_A^2 = 1.32\ GeV^2$. The HPW measurements from Ref. 11 are indicated by the shaded bands. The point at $\sin^2\theta_W = 0.4$, the Weinberg angle favored by deep-inelastic scattering data, is the CIR measurement also from Ref. 11. (b) The ratio $R_{el}^{\bar{\nu}}$ of elastic to quasielastic antineutrino-proton cross sections in the Weinberg-Salam model.

Fig. 12: Same as Fig. 11, for the vector model. In this instance, the preferred value of the Weinberg angle is $\sin^2\theta_W = 0.5$.

Fig. 13: Same as Fig. 11, for Gürsey-Sikivie model (B). In this instance, the preferred value of the Weinberg angle is $\sin^2\theta_W = 0.4$.

Fig. 14: Same as Fig. 11, for Gürsey-Sikivie model (C). In this instance, the preferred value of the Weinberg angle is $\sin^2\theta_W = 0.4$.

Fig. 15: (a) Energy dependence of the cross sections for quasielastic neutrino and antineutrino scattering. The lower limit of each band corresponds to an axial form factor with $M_A^2 = 0.71\ GeV^2$; the upper limit is for $M_A^2 = 1.32\ GeV^2$. (b) Energy dependence of the cross sections for elastic neutrino (solid curves) and antineutrino (dashed curves)-proton scattering in the Weinberg-Salam model with

$\sin^2 \theta_W = 0.4$. The lower two curves are for $M_A^2 = 0.71$ GeV^2; the upper two correspond to $M_A^2 = 1.32$ GeV^2.

Fig. 16: Differential cross sections for elastic νp scattering and for quasielastic neutrino scattering in the Weinberg-Salam model with $\sin^2 \theta_W = 0.4$. Solid curves correspond to an axial form factor with $M_A^2 = 0.71$ GeV^2; the dashed curves are for $M_A^2 = 1.32$ GeV^2. Data are from the HPW experiment, Ref. 11.

Fig. 17: Same as Fig. 16, for the vector model with $\sin^2 \theta_W = 0.5$.

Fig. 18: Same as Fig. 16, for Gürsey-Sikivie model (B), with $\sin^2 \theta_W = 0.4$.

Fig. 19: Same as Fig. 16, for Gürsey-Sikivie model (C), with $\sin^2 \theta_W = 0.4$.

Fig. 20: Differential cross sections for elastic νn and $\bar{\nu} n$ scattering in the Weinberg-Salam model with $\sin^2 \theta_W = 0.4$. Solid and dotted curves correspond to an axial form factor with $M_A^2 = 0.71$ GeV^2; the dashed and dot-dashed curves are for $M_A^2 = 1.32$ GeV^2.

Fig. 21: Differential cross sections for elastic $\bar{\nu} p$ scattering and for quasielastic antineutrino scattering in the Weinberg-Salam model with $\sin^2 \theta_W = 0.4$. Solid curves correspond to an axial form factor with $M_A^2 = 0.71$ GeV^2; the dashed curves are for $M_A^2 = 1.32$ GeV^2. Data are from the HPW experiment, Ref. 11.

Fig. 22: Same as Fig. 21, for the vector model. In this instance, the preferred value of the Weinberg angle is $\sin^2 \theta_W = 0.5$.

Fig. 23: Same as Fig. 21, for Gürsey-Sikivie model (B). In this instance, the preferred value of the Weinberg angle is $\sin^2 \theta_W = 0.4$.

Fig. 24: Same as Fig. 21, for Gürsey-Sikivie model (C). In this instance, the preferred value of the Weinberg angle is $\sin^2 \theta_W = 0.4$.

Fig. 25: The ratio of flux averaged antineutrino to neutrino cross sections, $\sigma(\bar{\nu}p \to \bar{\nu}p)/\sigma(\nu p \to \nu p)$, for the HPW cuts, as a function of $\sin^2 \theta_W$. The curves are for the Weinberg-Salam (W-S), vector (V), and Gürsey-Sikivie (G-S) (B) and (C) models. The solid and dashed curves correspond to an axial vector form factor with $M_A^2 = 0.71$ GeV^2 and 1.32 GeV^2, respectively. The HPW experiment has obtained the result $\sigma(\bar{\nu}p \to \bar{\nu}p)/\sigma(\nu p \to \nu p) = 0.35 \pm 0.2$. [Ref. 11].

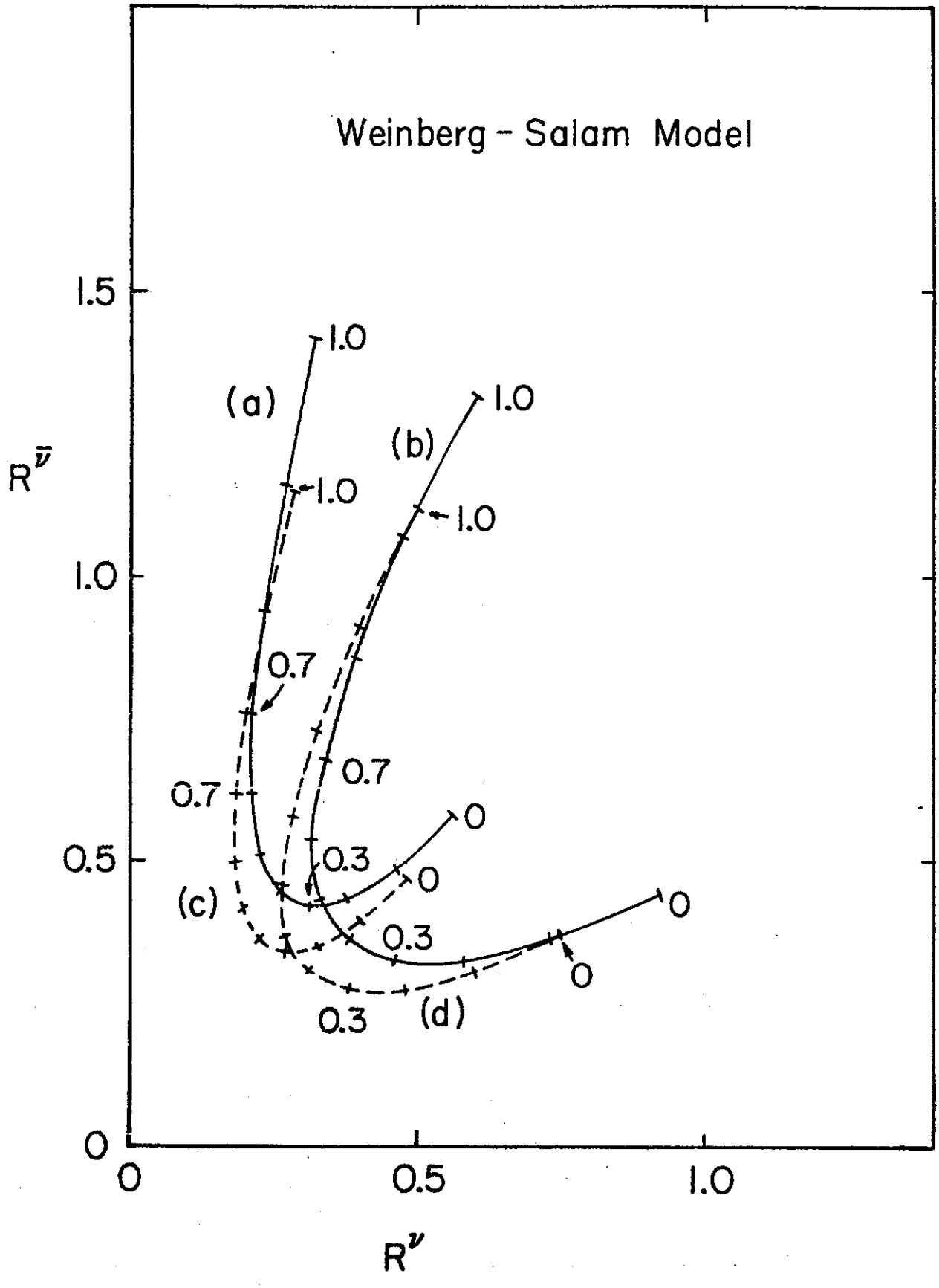
Weinberg - Salam Model
1.5
1.0
0.5
0
0
0.5
1.0
$R^{\bar{\nu}}$
R^{ν}
(a)
(b)
(c)
(d)
1.0
1.0
1.0
1.0
0.7
0.7
0.7
0.3
0.3
0.3
0
0
0
0

Fig. 1

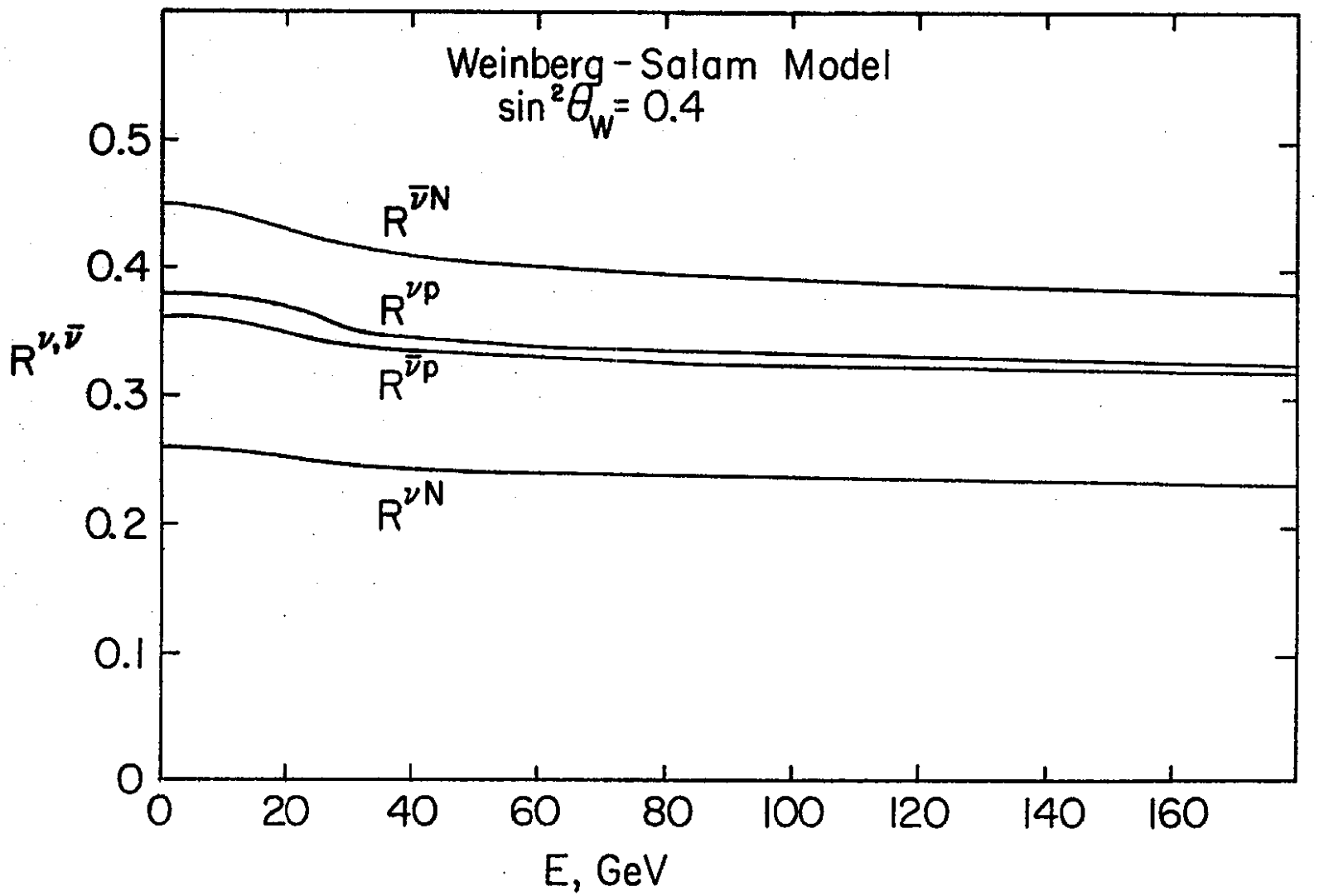
Weinberg - Salam Model
$\sin^2\theta_W = 0.4$
$R^{\nu,\bar{\nu}}$
$R^{\bar{\nu}N}$
$R^{\nu p}$
$R^{\bar{\nu}p}$
$R^{\nu N}$
0.5
0.4
0.3
0.2
0.1
0
0
20
40
60
80
100
120
140
160
E, GeV

Fig. 2

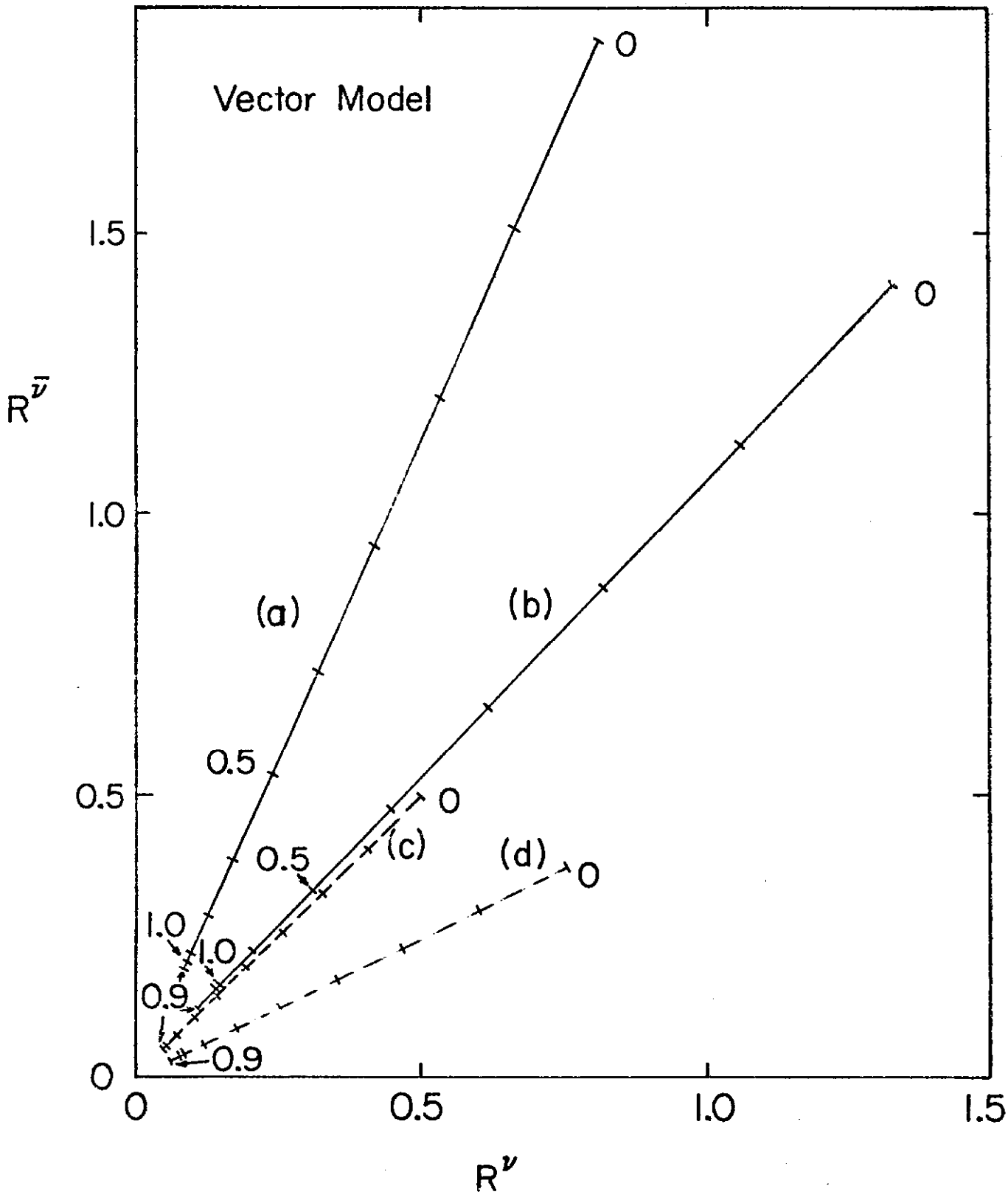
Vector Model
0
0
0.5
0
0.5
1.0
1.0
0.9
0.9
(a)
(b)
(c)
(d)
0
0.5
1.0
1.5
0
0.5
1.0
1.5
$R^{\bar{\nu}}$
R^{ν}

Fig. 3

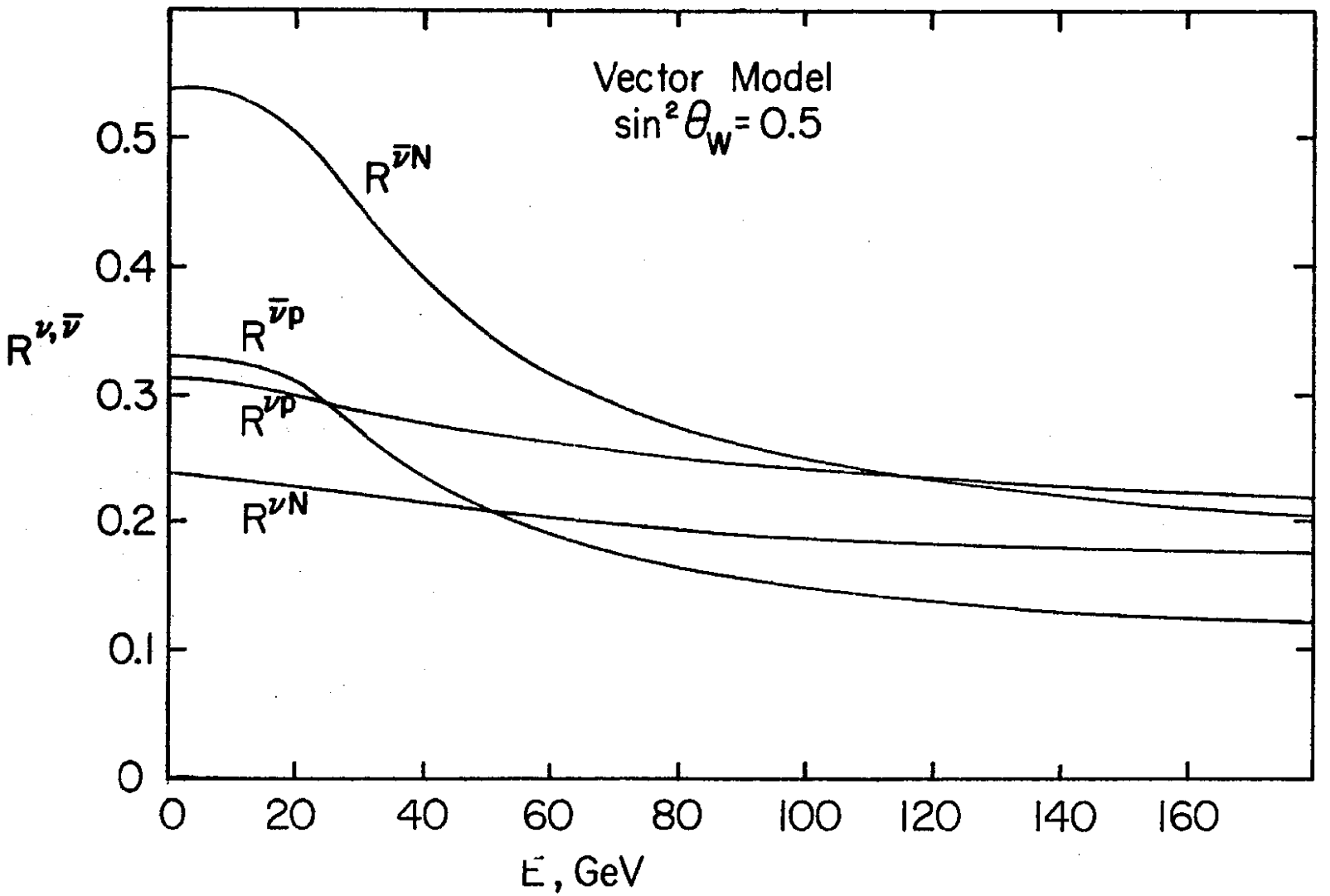
Vector Model
sin²θW = 0.5
R^ν̄N
R^ν̄p
R^νp
R^νN
R^ν,ν̄
0.5
0.4
0.3
0.2
0.1
0
0
20
40
60
80
100
120
140
160
E, GeV

Fig. 4

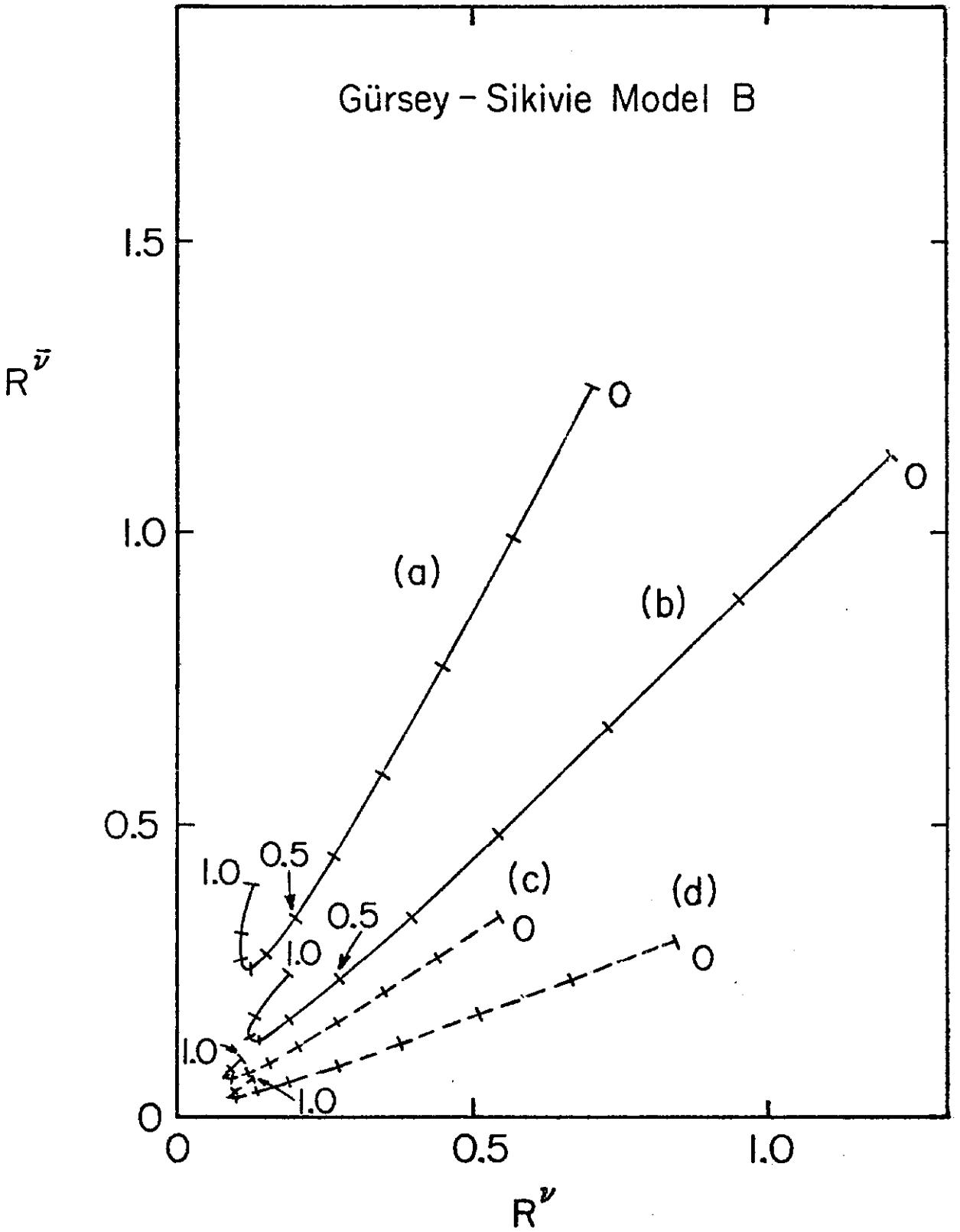
Gürsey – Sikivie Model B
1.5
1.0
0.5
0
0
0.5
1.0
$R^{\tilde{\nu}}$
R^{ν}
(a)
(b)
(c)
(d)
0
0
0
0
0.5
1.0
0.5
1.0
1.0
1.0

Fig. 5

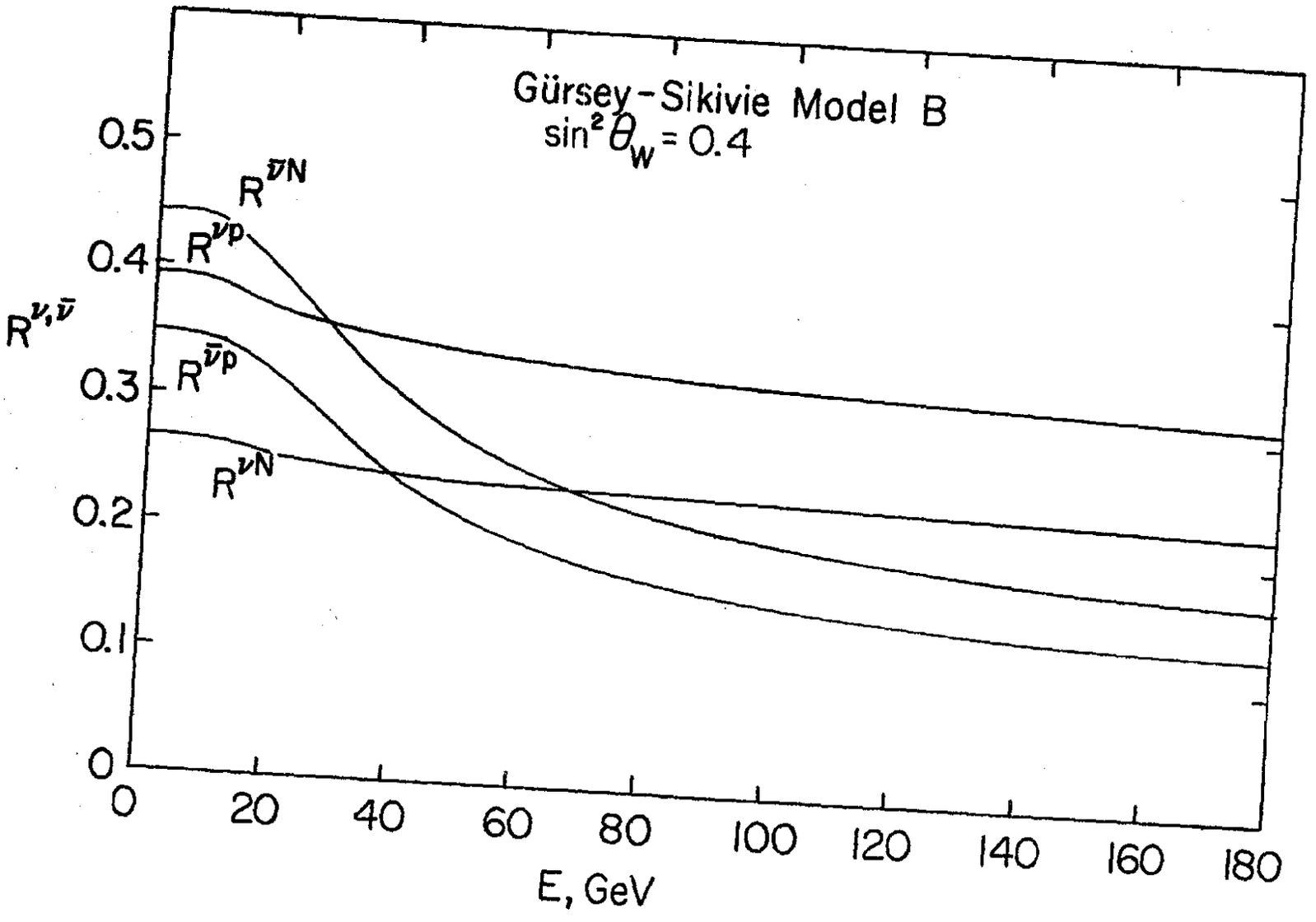
Gürsey-Sikivie Model B
$\sin^2\theta_W = 0.4$
$R^{\bar{\nu}N}$
$R^{\nu p}$
$R^{\bar{\nu}p}$
$R^{\nu N}$
$R^{\nu,\bar{\nu}}$
0.5
0.4
0.3
0.2
0.1
0
0
20
40
60
80
100
120
140
160
180
E, GeV

Fig. 6

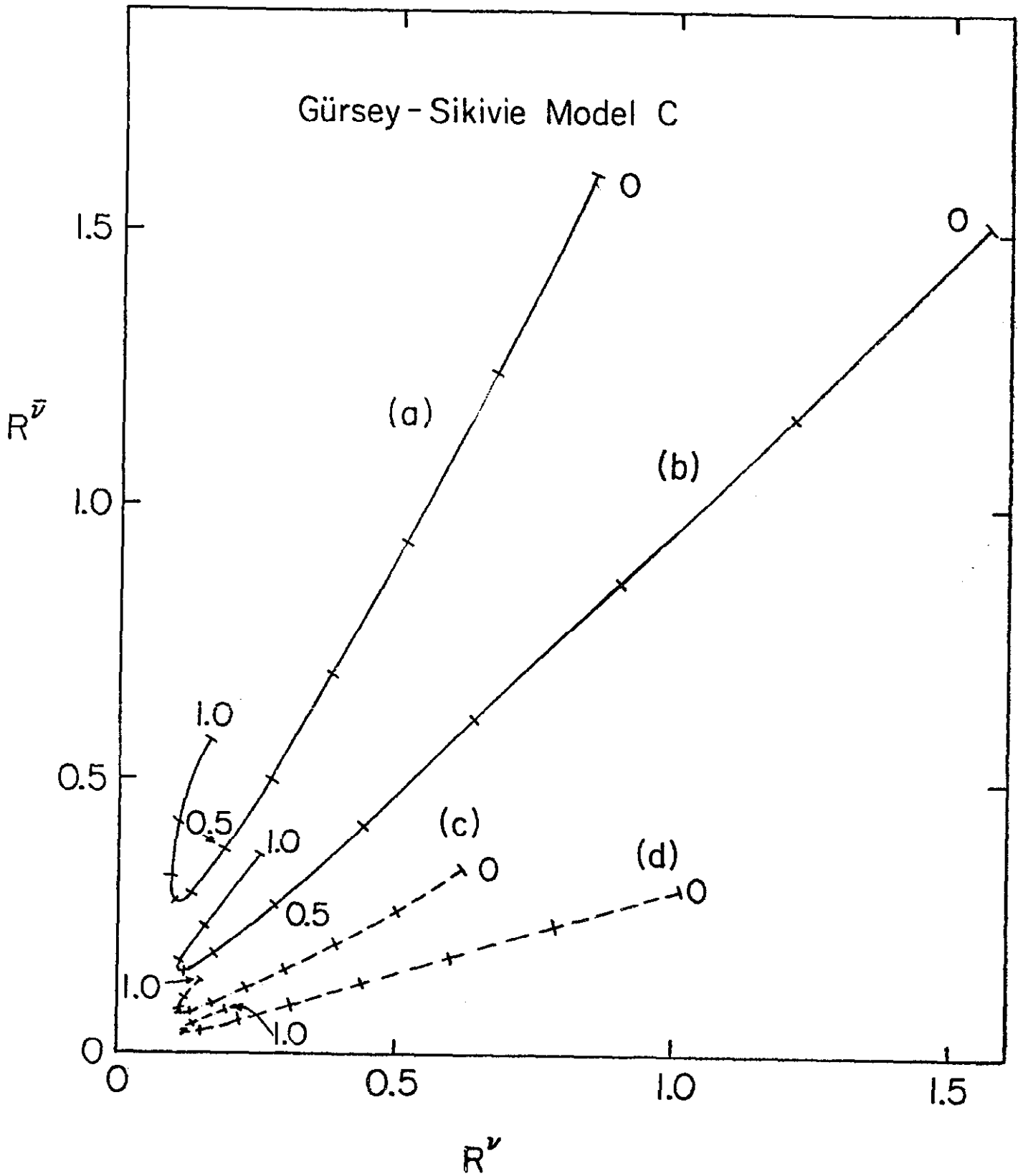
Gürsey - Sikivie Model C
0
0
(a)
(b)
1.0
0.5
1.0
(c)
0
(d)
0
0.5
1.0
1.0
1.0
0.5
0
0
0.5
1.0
1.5
$R^{\bar{\nu}}$
R^{ν}

Fig. 7

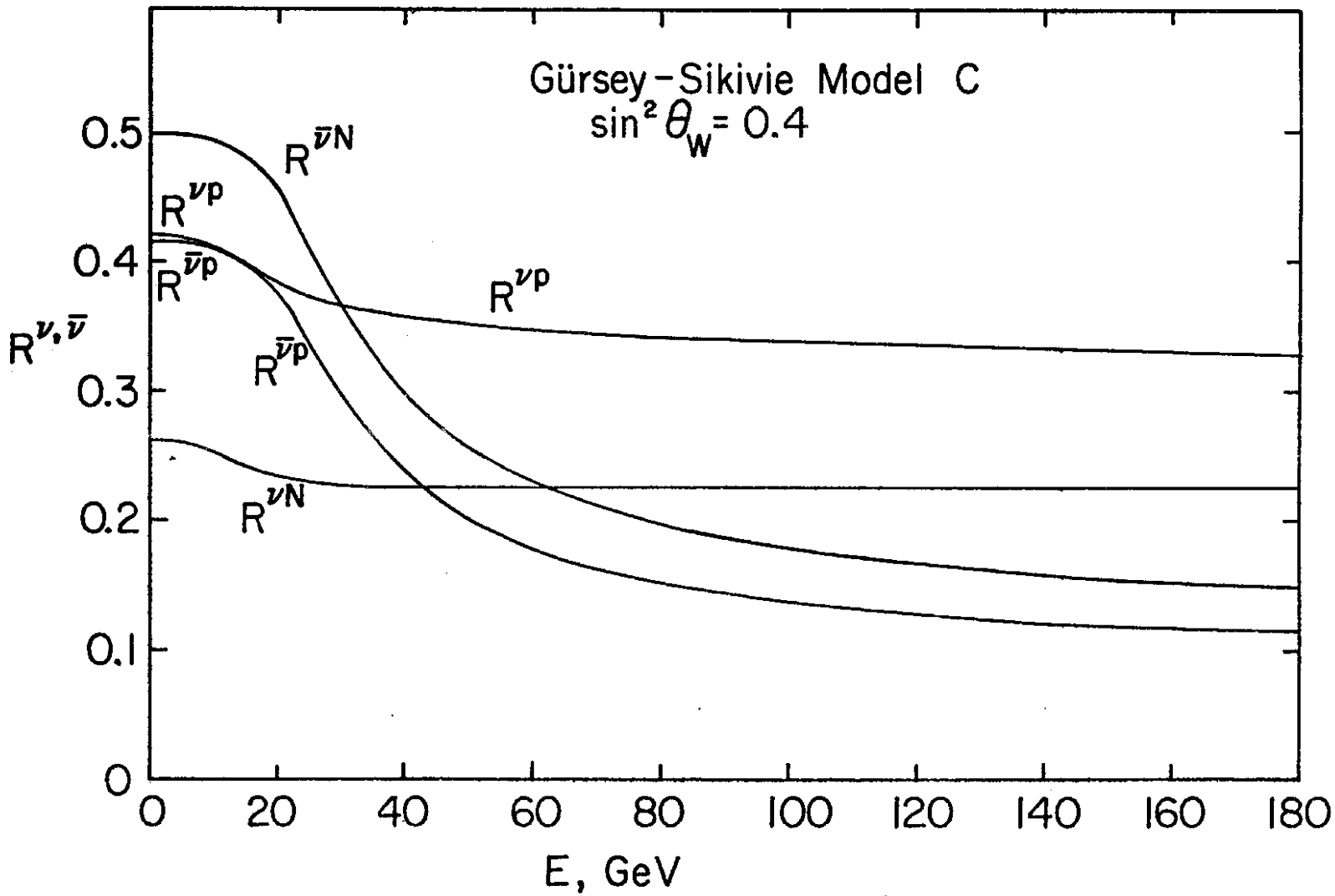
Gürsey-Sikivie Model C
$\sin^2\theta_W = 0.4$
$R^{\bar{\nu}N}$
$R^{\nu p}$
$R^{\bar{\nu}p}$
$R^{\nu p}$
$R^{\bar{\nu}p}$
$R^{\nu N}$
$R^{\nu,\bar{\nu}}$
0.5
0.4
0.3
0.2
0.1
0
0
20
40
60
80
100
120
140
160
180
E, GeV

Fig. 8

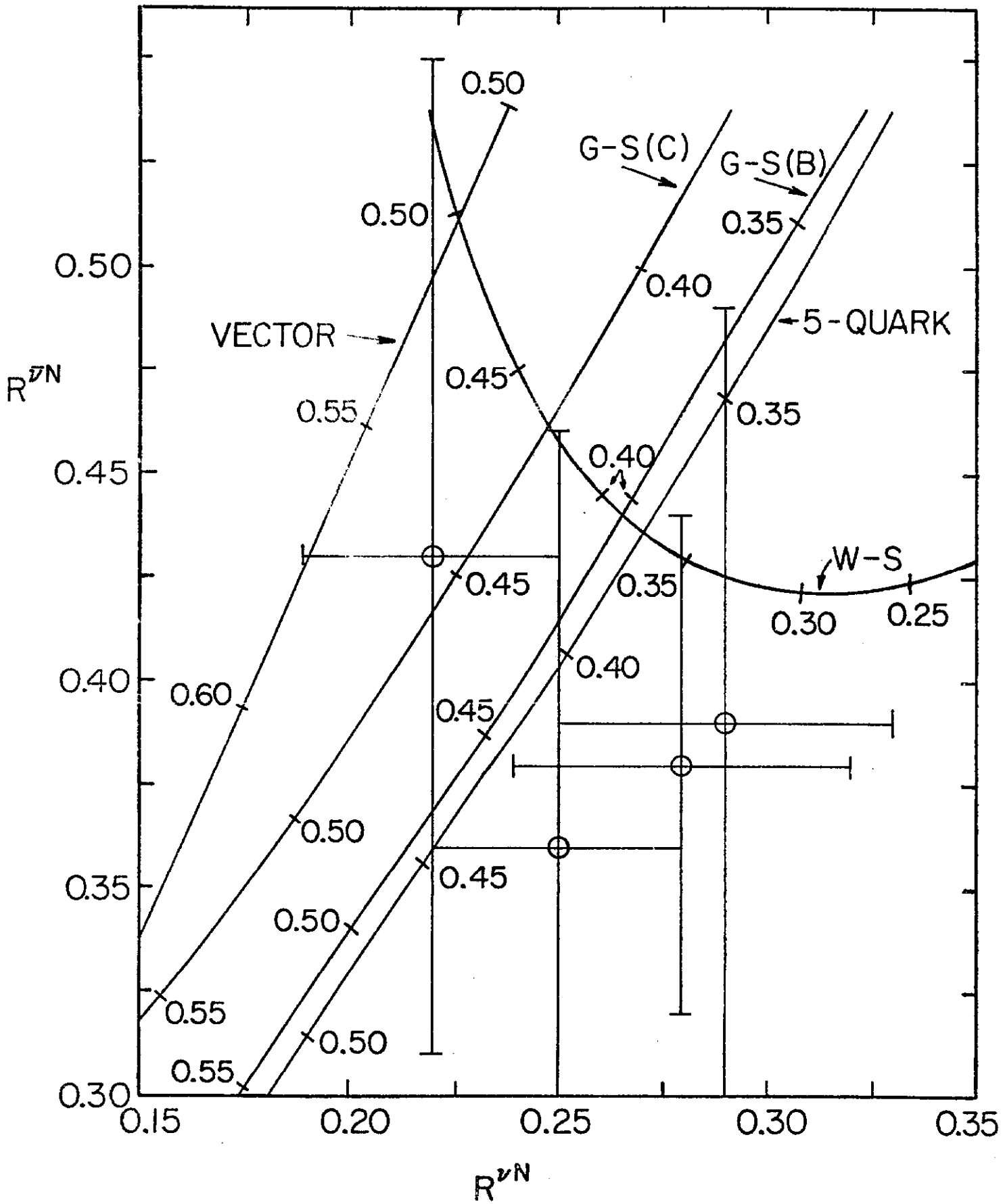
G-S(C)
G-S(B)
VECTOR
5-QUARK
W-S
0.50
0.55
0.60
0.45
0.40
0.35
0.30
0.25
0.50
0.45
0.40
0.35
0.30
0.15
0.20
0.25
0.30
0.35
$R^{\bar{\nu}N}$
$R^{\nu N}$

Fig. 9

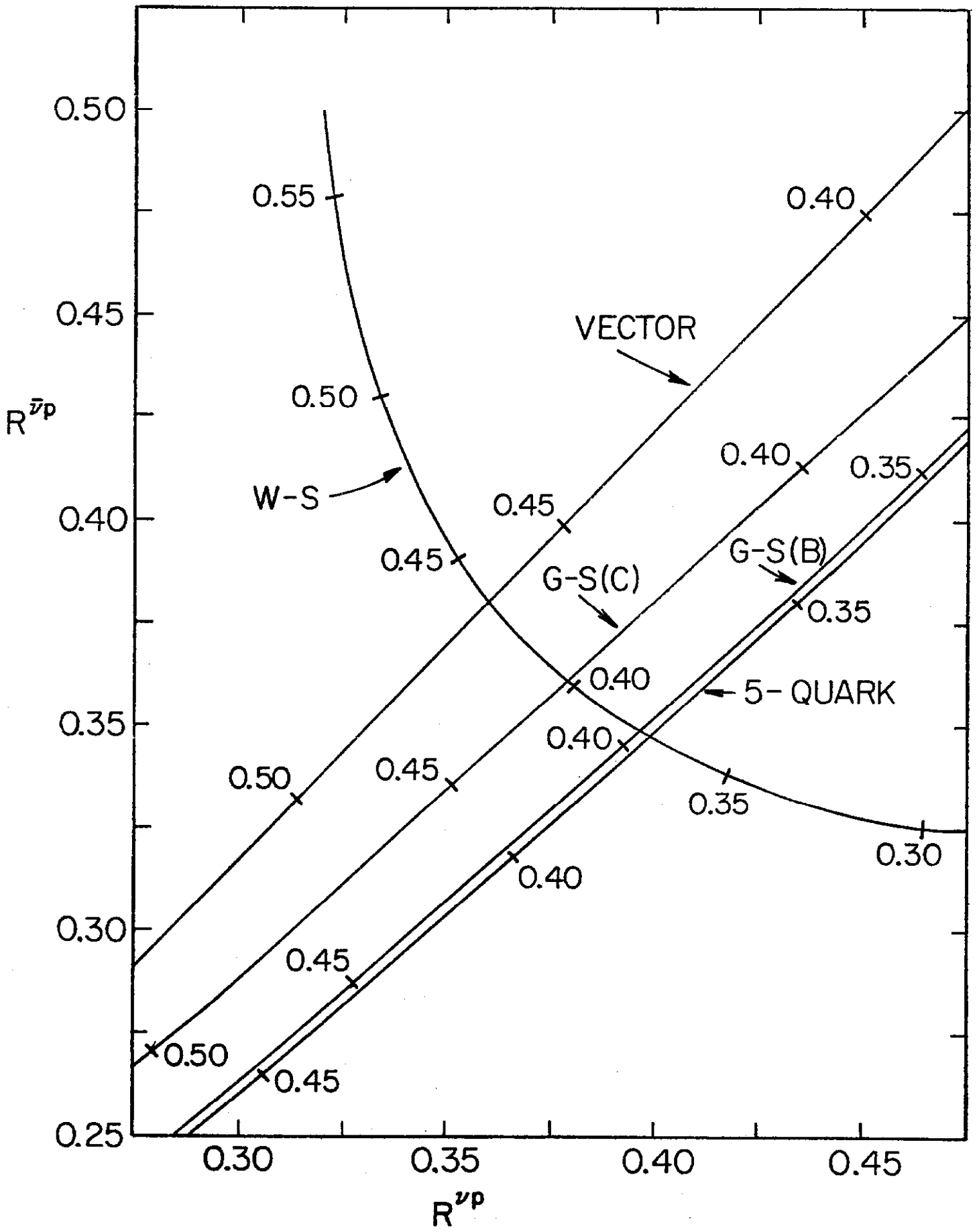
0.50
0.45
0.40
0.35
0.30
0.25
$R^{\bar{\nu}p}$
0.30
0.35
0.40
0.45
$R^{\nu p}$
0.55
0.50
0.45
0.40
0.35
0.30
VECTOR
W-S
G-S(C)
G-S(B)
5- QUARK

Fig. 10

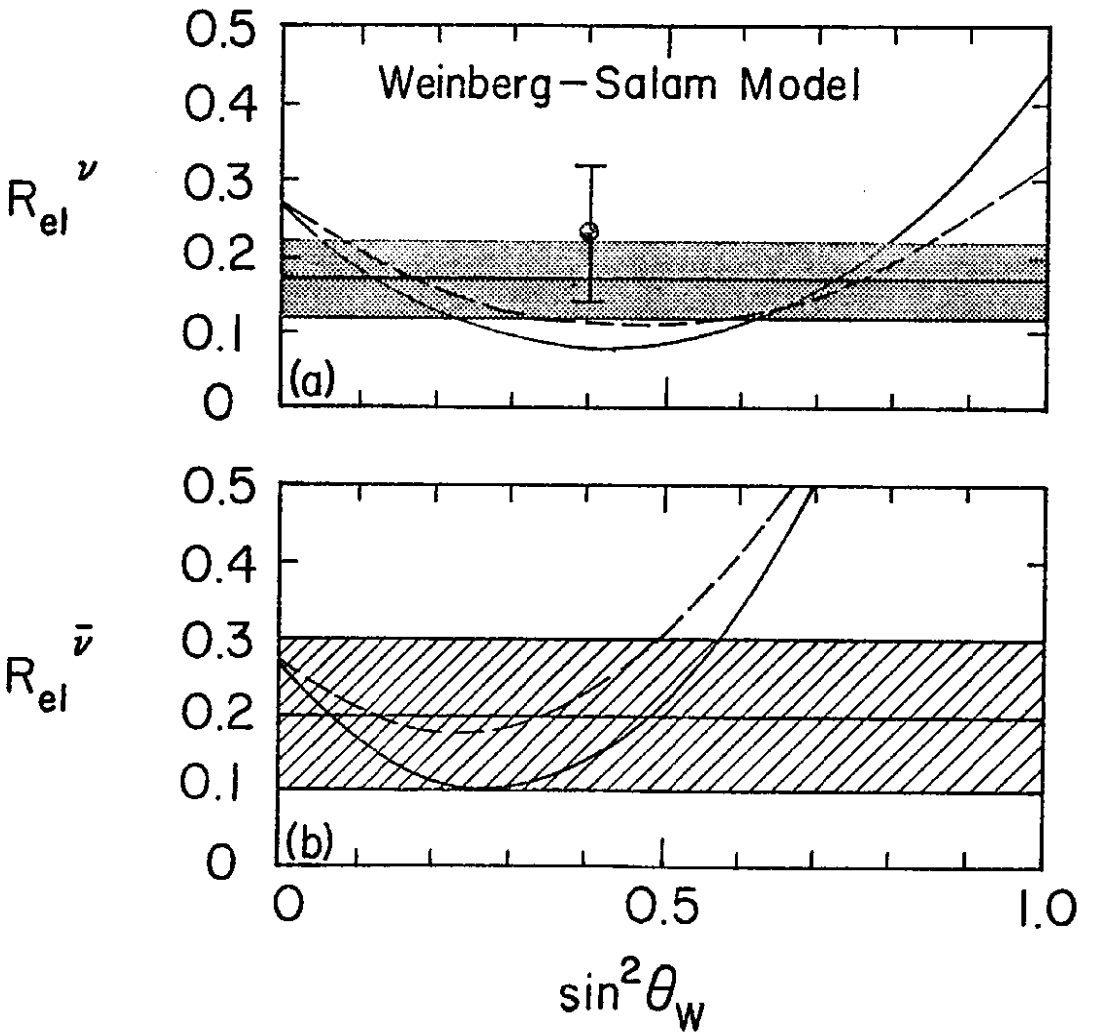
Weinberg–Salam Model
R_{el}^{ν}
$R_{el}^{\bar{\nu}}$
0.5
0.4
0.3
0.2
0.1
0
(a)
(b)
0
0.5
1.0
$\sin^2\theta_W$

Fig. 11

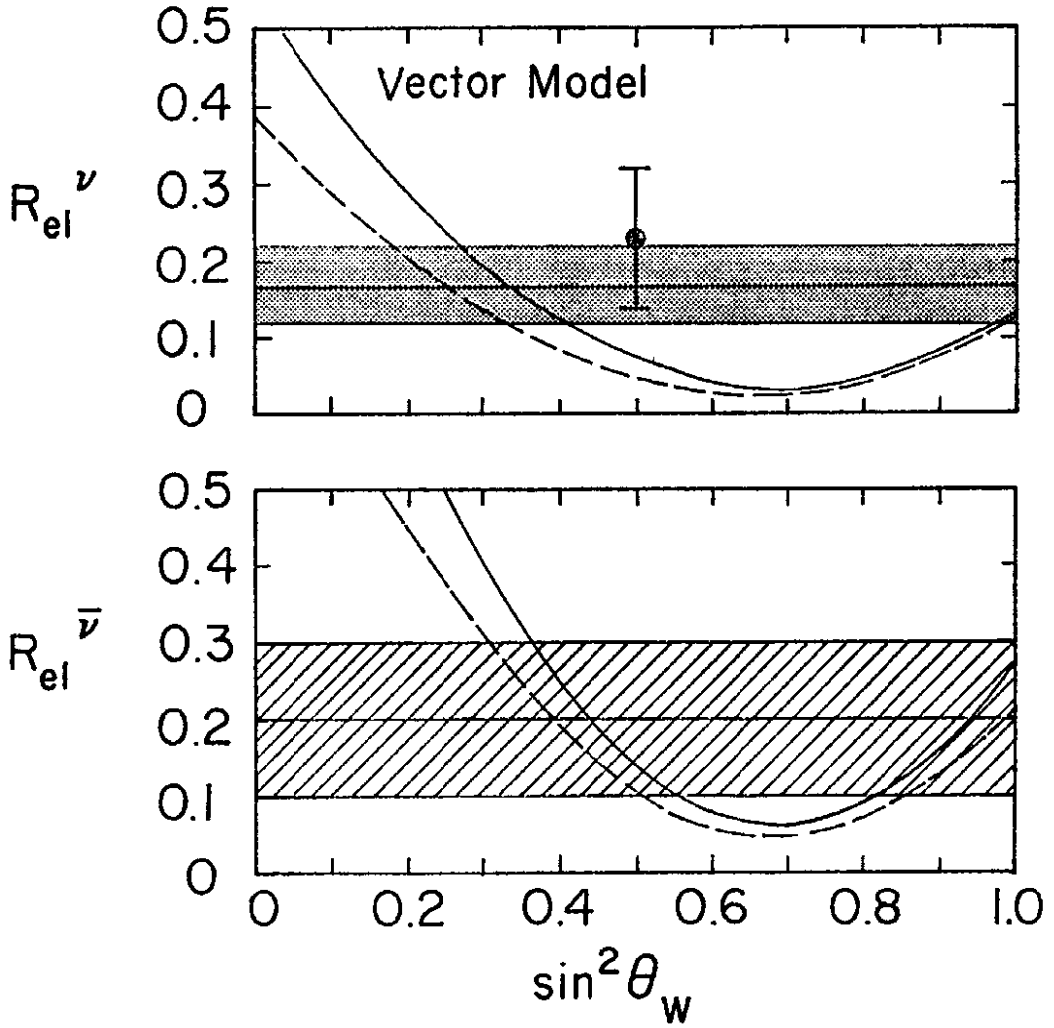
Vector Model
R_{el}^{ν}
$R_{el}^{\bar{\nu}}$
0.5
0.4
0.3
0.2
0.1
0
0
0.2
0.4
0.6
0.8
1.0
$\sin^2\theta_W$

Fig. 12

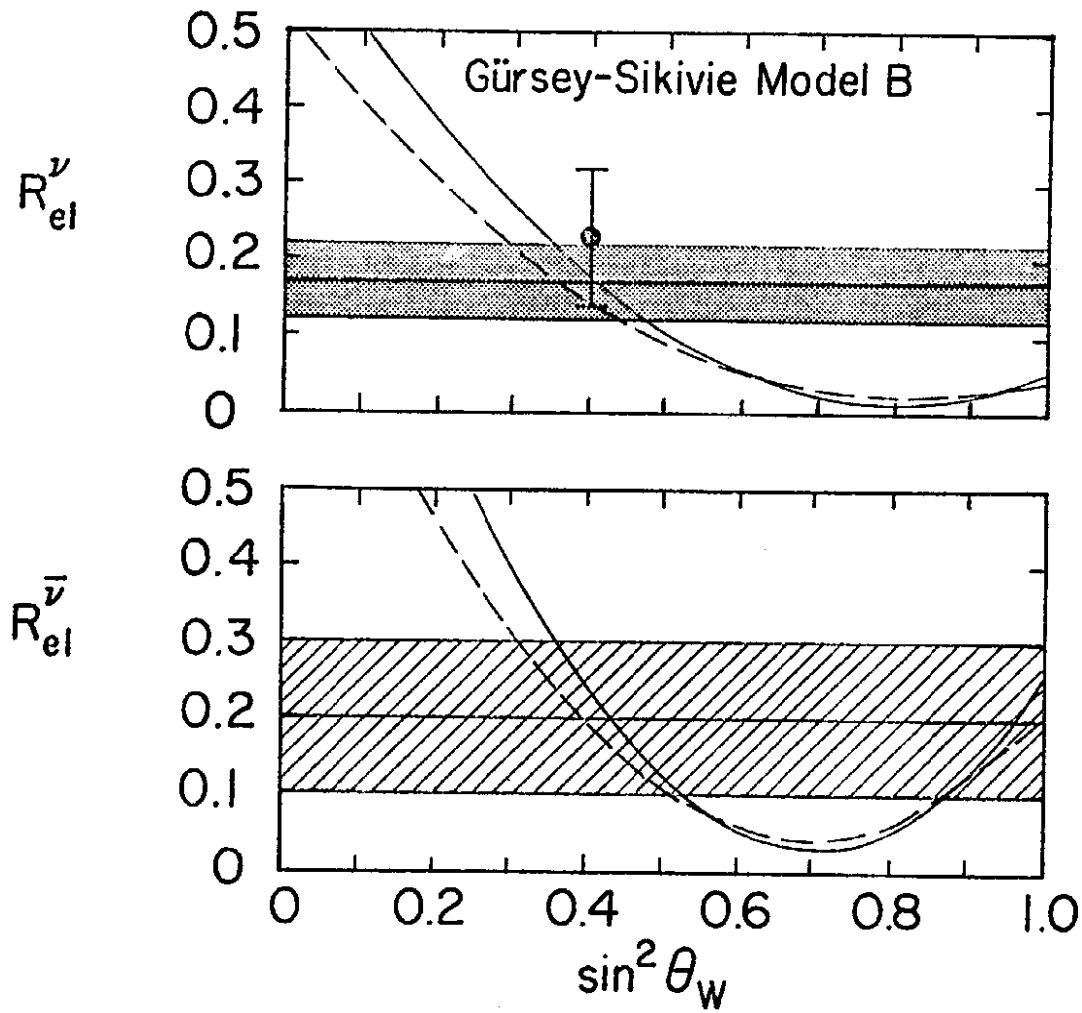
Gürsey-Sikivie Model B
R_{el}^{ν}
$R_{el}^{\bar{\nu}}$
0.5
0.4
0.3
0.2
0.1
0
0
0.2
0.4
0.6
0.8
1.0
$\sin^2\theta_W$

Fig. 13

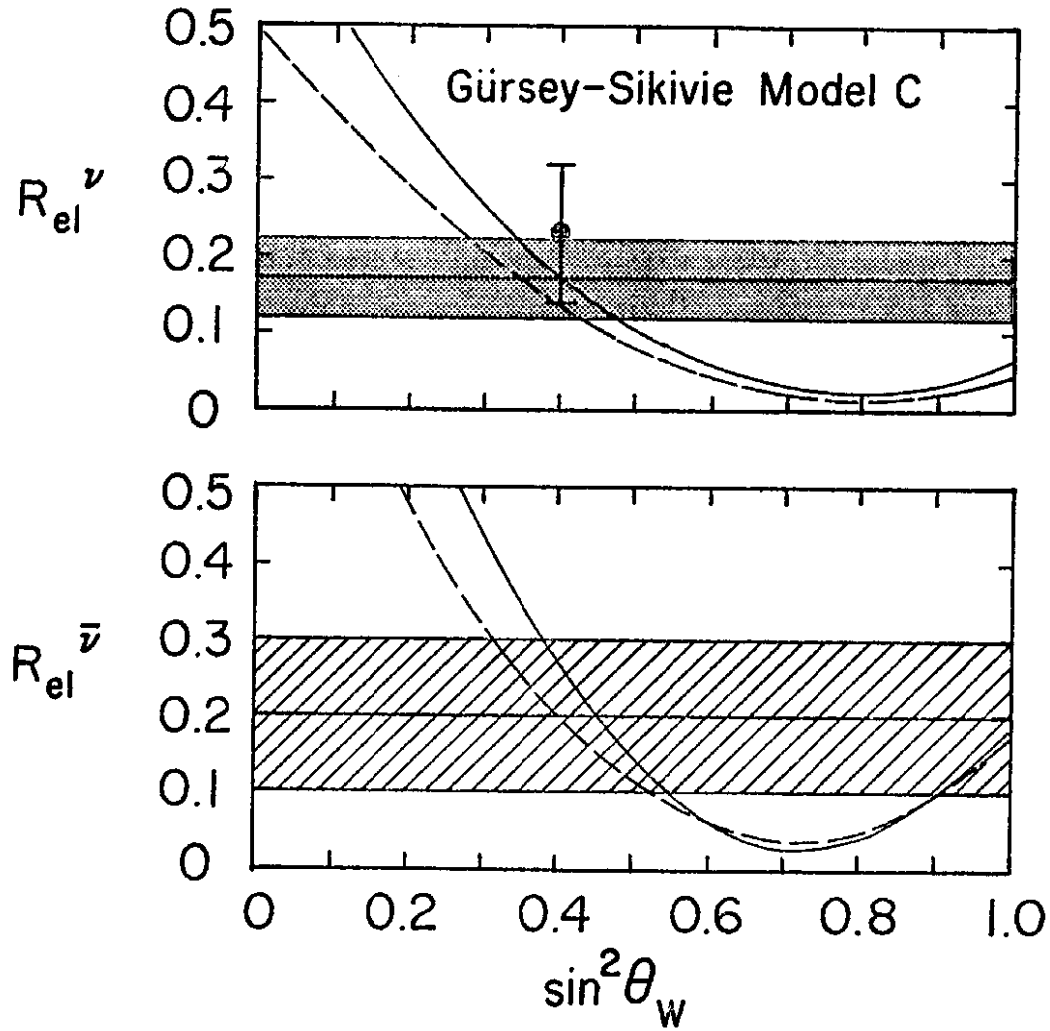
Gürsey-Sikivie Model C
R_{el}^{ν}
$R_{el}^{\bar{\nu}}$
0.5
0.4
0.3
0.2
0.1
0
0
0.2
0.4
0.6
0.8
1.0
$\sin^2\theta_W$

Fig. 14

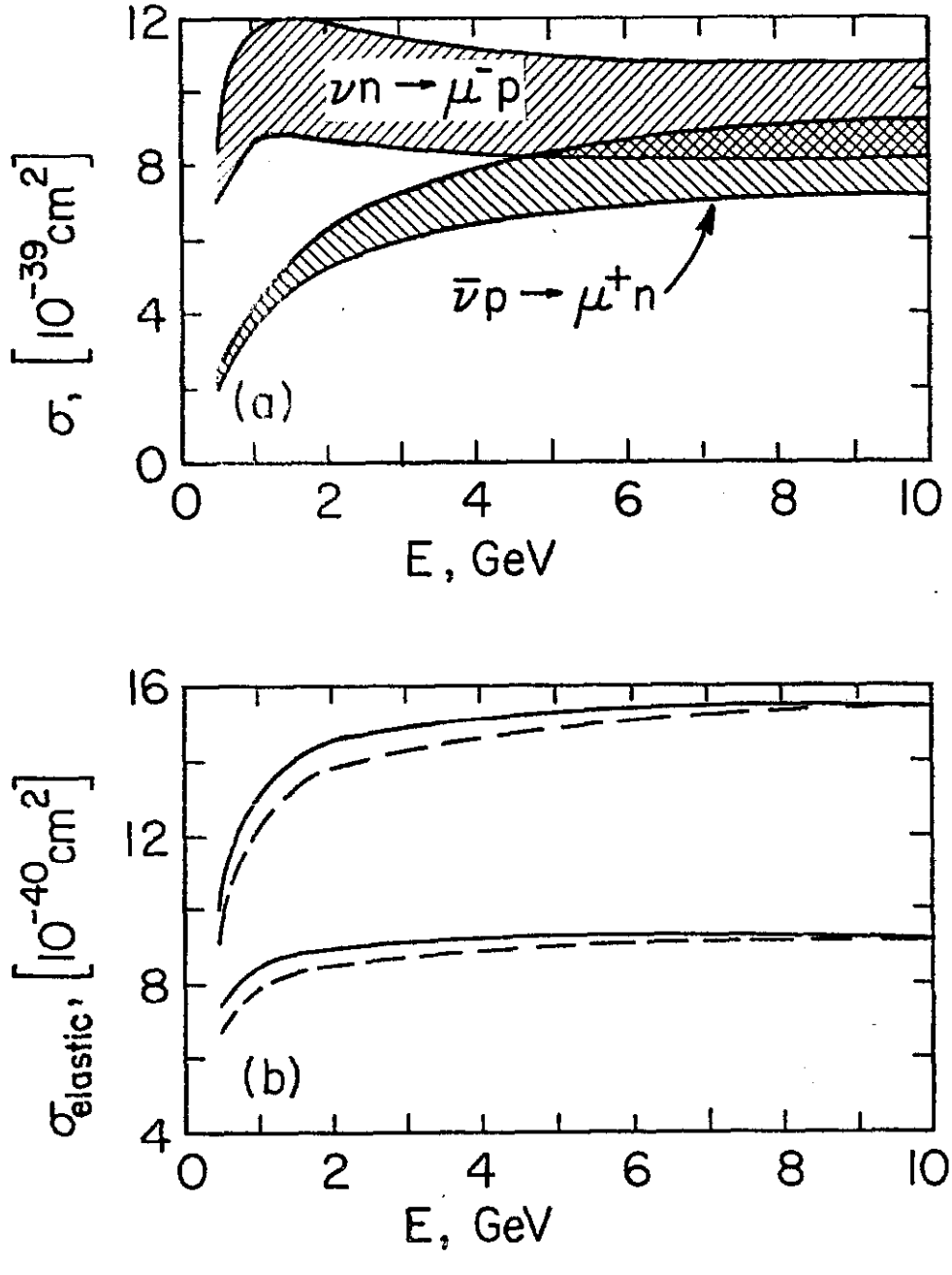
12
8
4
0
0
2
4
6
8
10
σ, [10^-39 cm^2]
νn → μ⁻p
ν̄p → μ⁺n
(a)
E, GeV
16
12
8
4
σelastic, [10^-40 cm^2]
(b)
E, GeV

Fig. 15

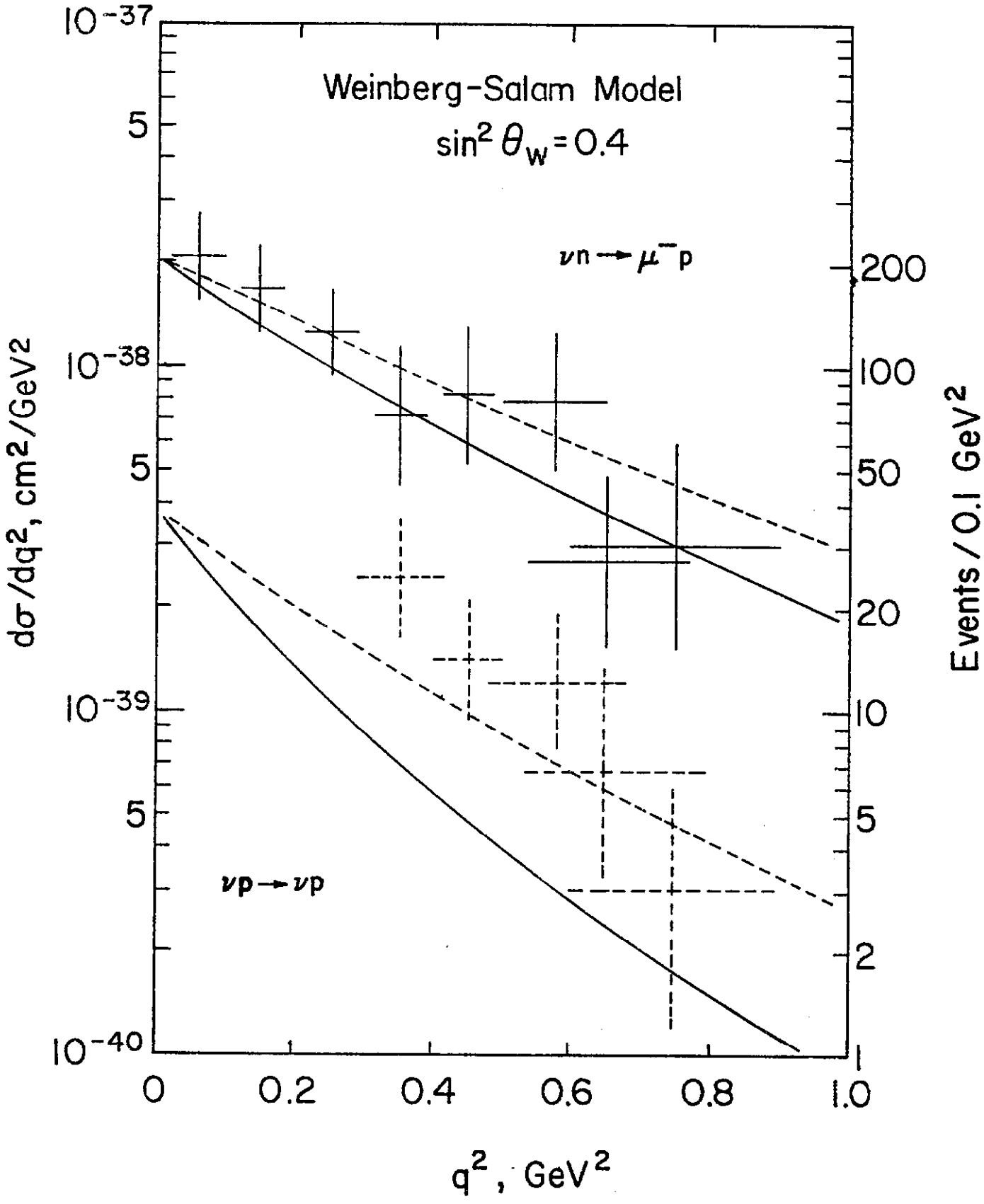
Weinberg-Salam Model
$\sin^2\theta_W = 0.4$
$\nu n \rightarrow \mu^- p$
$\nu p \rightarrow \nu p$
$d\sigma/dq^2$, cm^2/GeV^2
Events / 0.1 GeV^2
q^2, GeV^2
10^{-37}
5
10^{-38}
5
10^{-39}
5
10^{-40}
0
0.2
0.4
0.6
0.8
1.0
200
100
50
20
10
5
2
1

Fig. 16

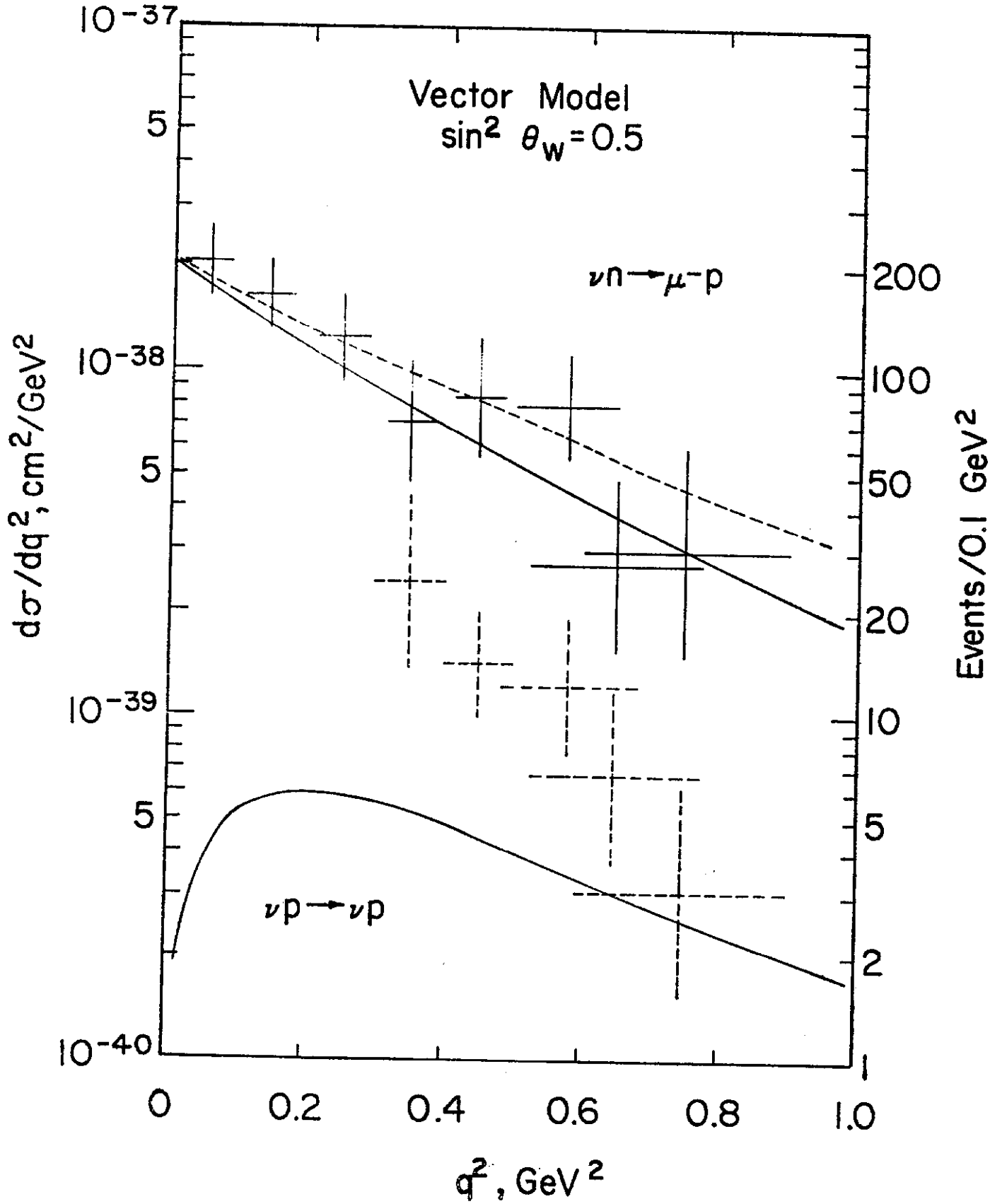
Vector Model
sin² θW = 0.5
νn → μ⁻p
νp → νp
dσ/dq², cm²/GeV²
Events/0.1 GeV²
q², GeV²
10⁻³⁷
5
10⁻³⁸
5
10⁻³⁹
5
10⁻⁴⁰
200
100
50
20
10
5
2
1
0
0.2
0.4
0.6
0.8
1.0

Fig. 17

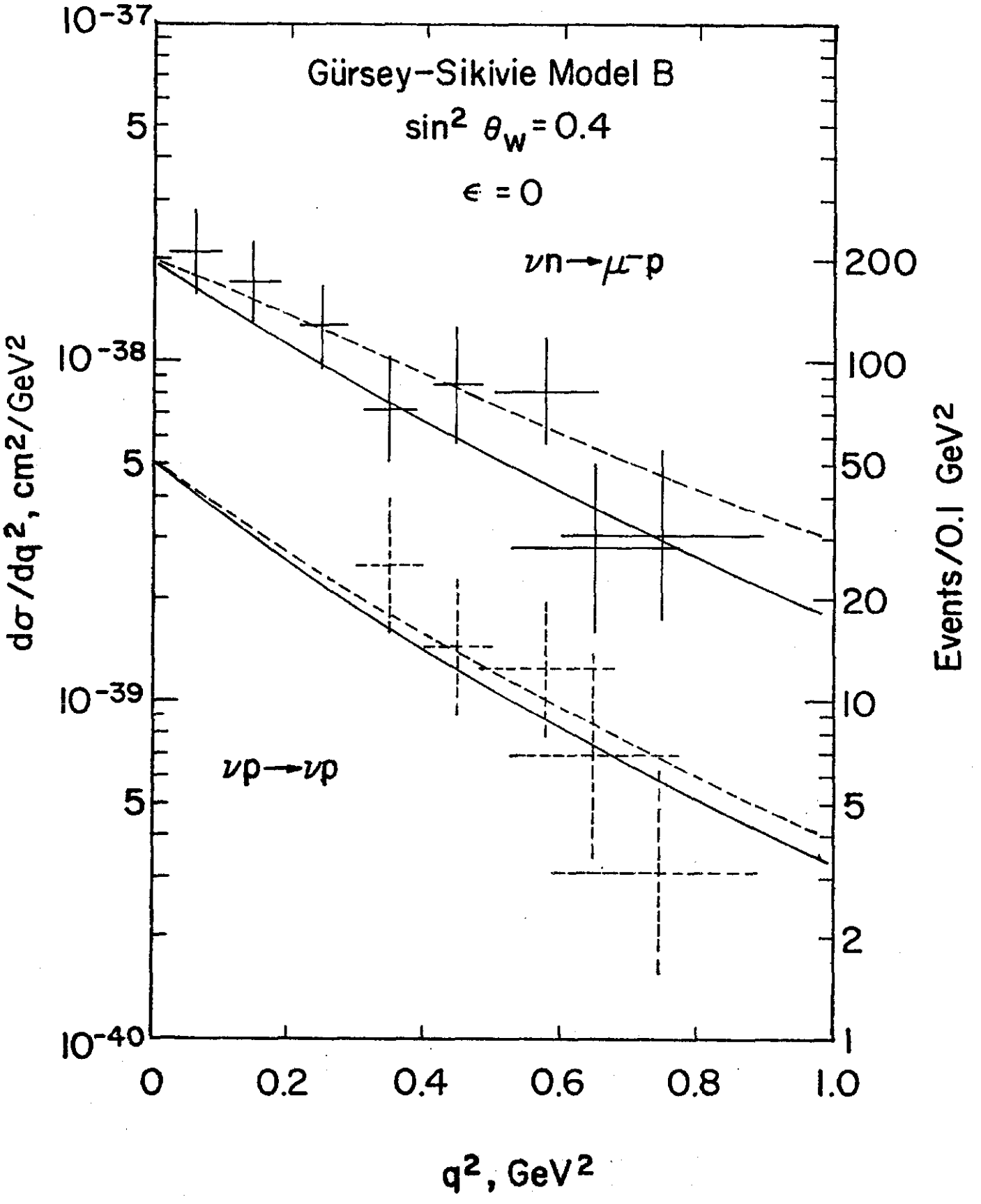
Gürsey-Sikivie Model B
sin² θW = 0.4
ϵ = 0
νn→μ⁻p
νp→νp
dσ/dq², cm²/GeV²
Events/0.1 GeV²
q², GeV²
10⁻³⁷
5
10⁻³⁸
5
10⁻³⁹
5
10⁻⁴⁰
200
100
50
20
10
5
2
1
0
0.2
0.4
0.6
0.8
1.0

Fig. 18

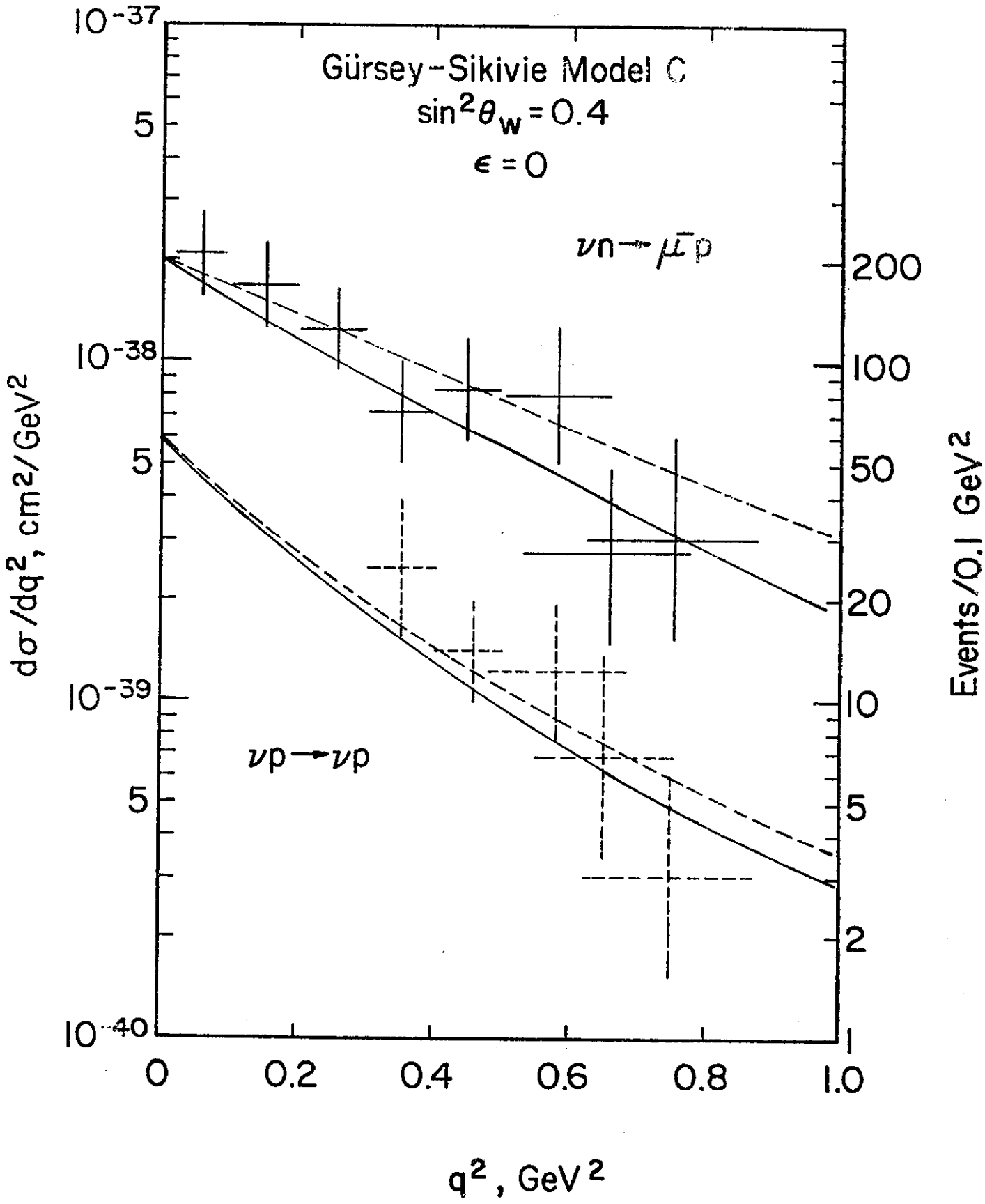
Gürsey-Sikivie Model C
$\sin^2\theta_w = 0.4$
$\epsilon = 0$
$\nu n \to \mu^- p$
$\nu p \to \nu p$
$d\sigma/dq^2$, cm^2/GeV^2
Events/0.1 GeV^2
q^2, GeV^2
10^{-37}
5
10^{-38}
5
10^{-39}
5
10^{-40}
200
100
50
20
10
5
2
1
0
0.2
0.4
0.6
0.8
1.0

Fig. 19

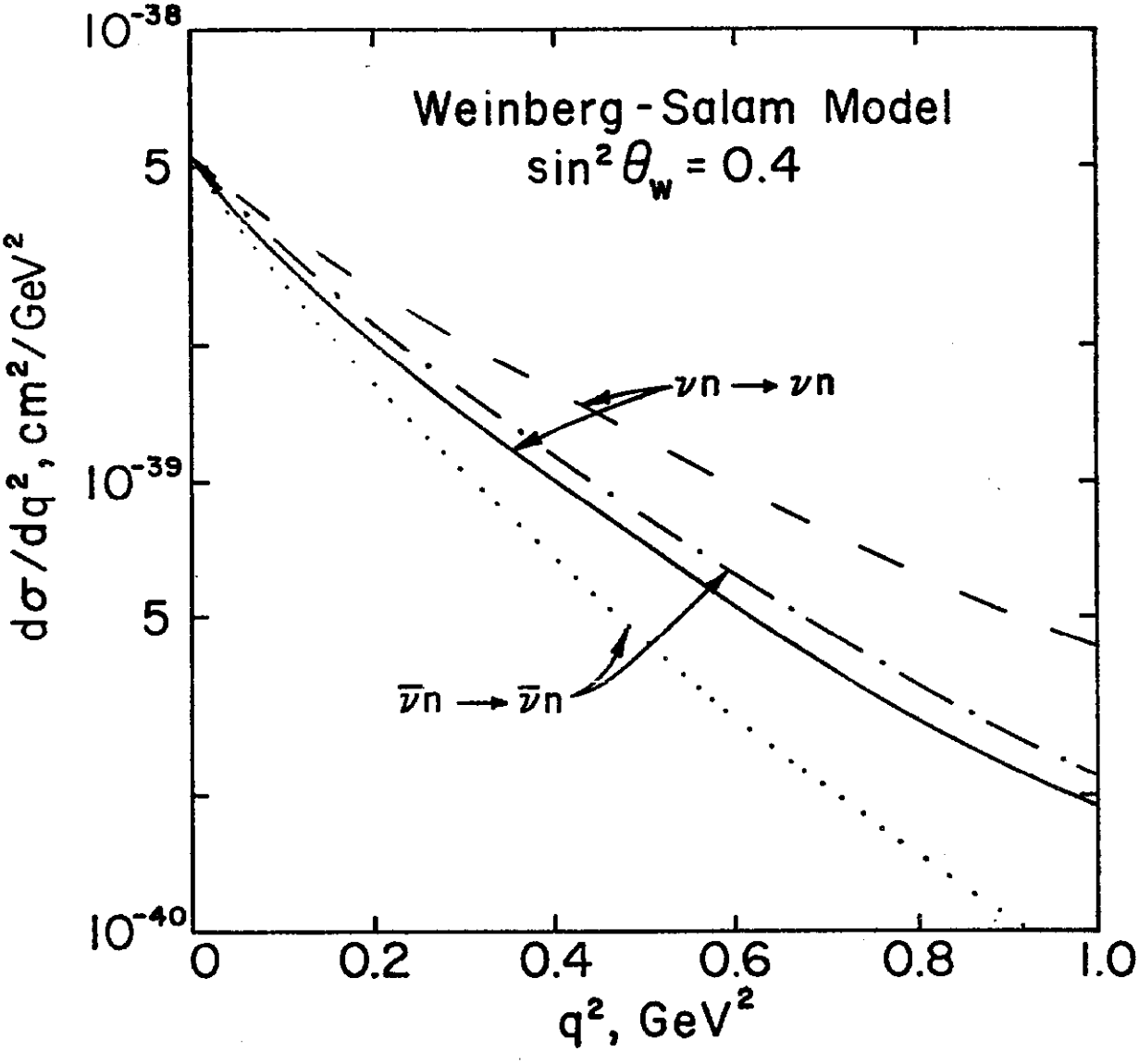
Weinberg - Salam Model
$\sin^2\theta_w = 0.4$
$\nu n \rightarrow \nu n$
$\bar{\nu} n \rightarrow \bar{\nu} n$
$d\sigma/dq^2$, cm^2/GeV^2
10^{-38}
5
10^{-39}
5
10^{-40}
0
0.2
0.4
0.6
0.8
1.0
q^2, GeV^2

Fig. 20

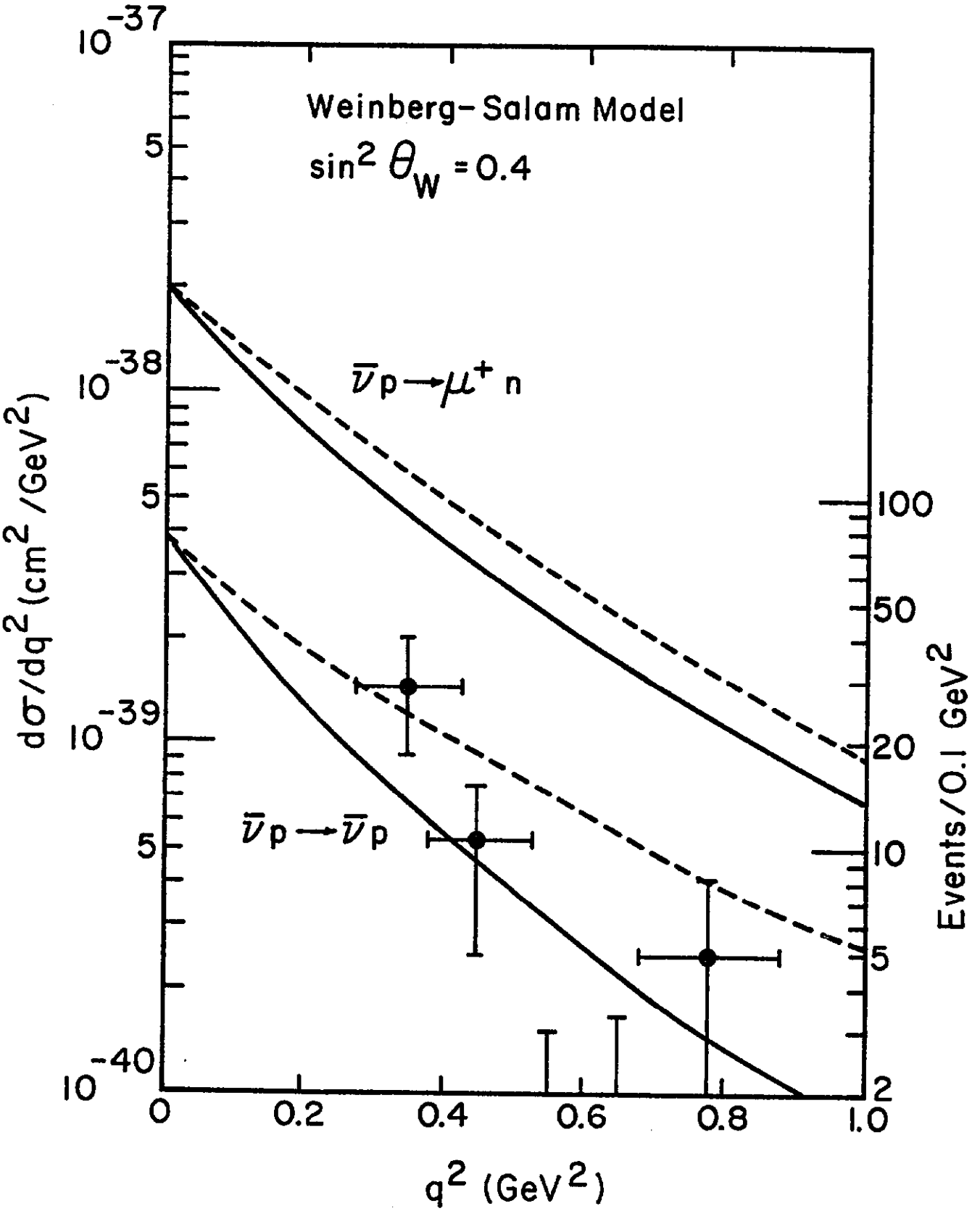
Weinberg-Salam Model
$\sin^2\theta_W = 0.4$
$\bar{\nu}p \to \mu^+ n$
$\bar{\nu}p \to \bar{\nu}p$
$d\sigma/dq^2$ (cm^2/GeV^2)
Events/0.1 GeV^2
q^2 (GeV^2)
10^{-37}
5
10^{-38}
5
10^{-39}
5
10^{-40}
0
0.2
0.4
0.6
0.8
1.0
100
50
20
10
5
2

Fig. 21

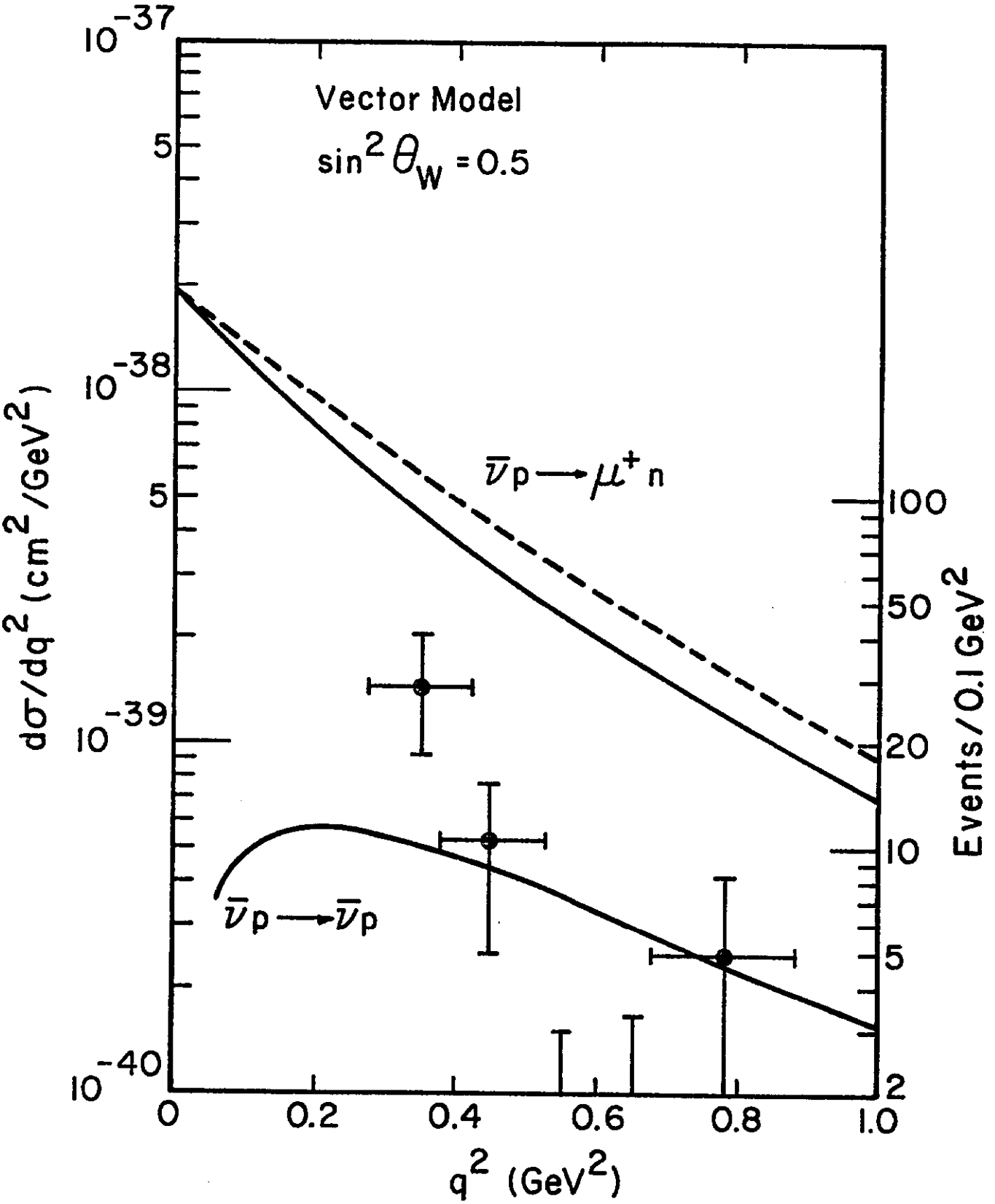
Vector Model
$\sin^2\theta_W = 0.5$
$\bar{\nu}p \rightarrow \mu^+ n$
$\bar{\nu}p \rightarrow \bar{\nu}p$
$d\sigma/dq^2$ (cm^2/GeV^2)
Events/0.1 GeV^2
q^2 (GeV^2)
10^{-37}
5
10^{-38}
5
10^{-39}
10^{-40}
0
0.2
0.4
0.6
0.8
1.0
100
50
20
10
5
2

Fig. 22

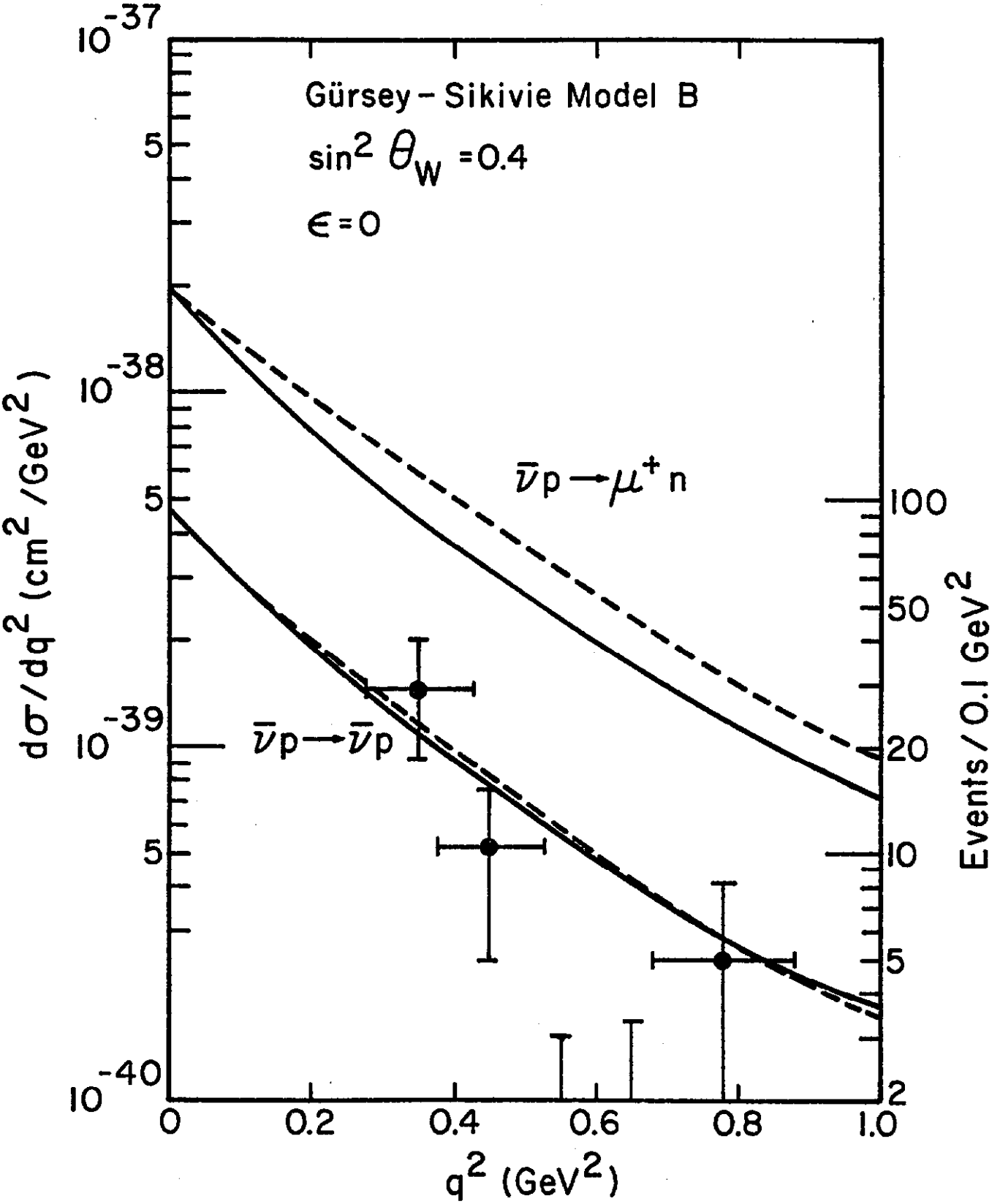
Gürsey – Sikivie Model B
sin² θW = 0.4
ϵ = 0
ν̄p → μ⁺n
ν̄p → ν̄p
dσ/dq² (cm²/GeV²)
Events / 0.1 GeV²
q² (GeV²)
10⁻³⁷
10⁻³⁸
10⁻³⁹
10⁻⁴⁰
5
5
5
0
0.2
0.4
0.6
0.8
1.0
100
50
20
10
5
2

Fig. 23

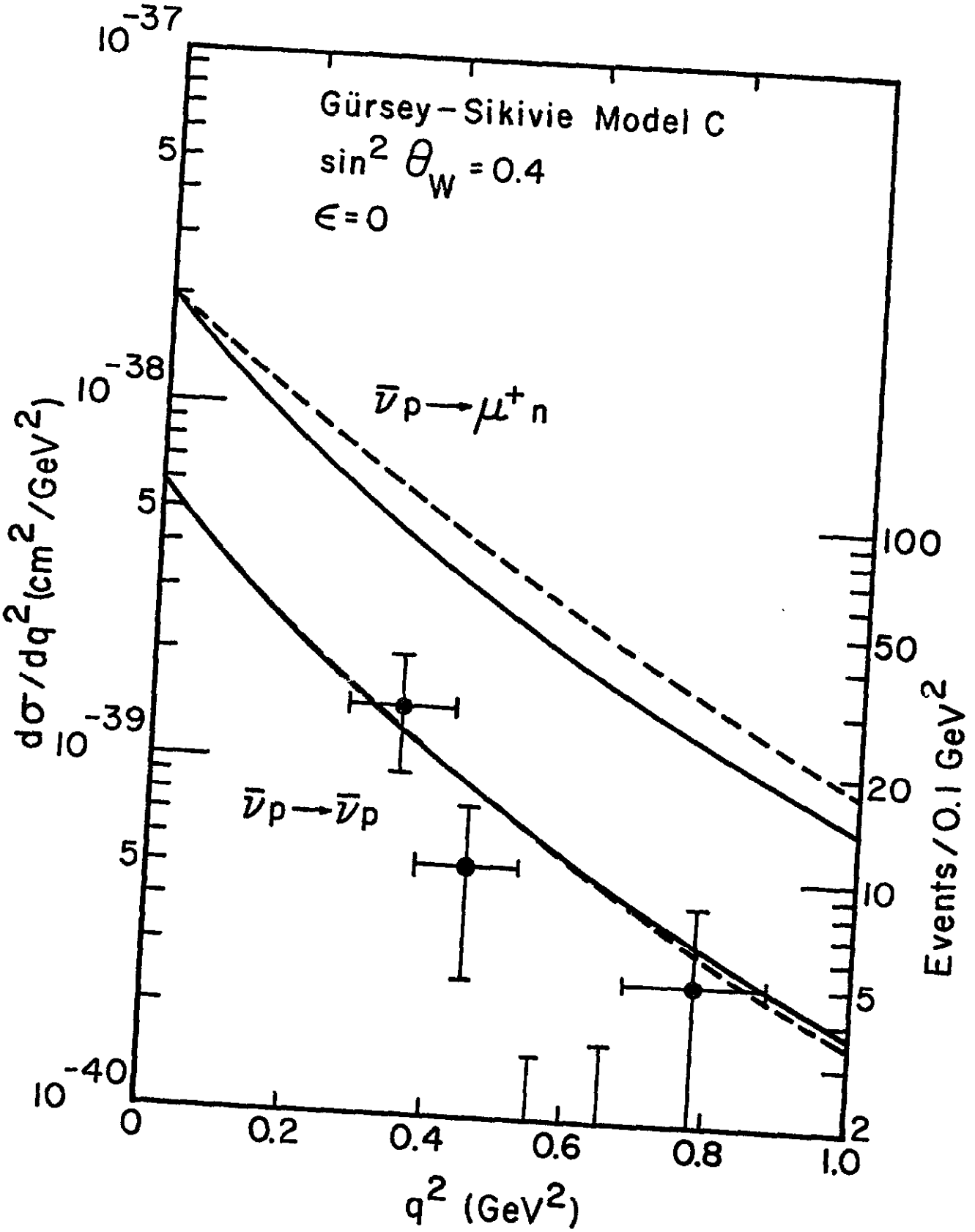
Gürsey-Sikivie Model C
sin² θW = 0.4
ϵ = 0
ν̄p → μ⁺n
ν̄p → ν̄p
dσ/dq² (cm²/GeV²)
Events/0.1 GeV²
q² (GeV²)
10⁻³⁷
10⁻³⁸
10⁻³⁹
10⁻⁴⁰
5
0
0.2
0.4
0.6
0.8
1.0
100
50
20
10
2

Fig. 24

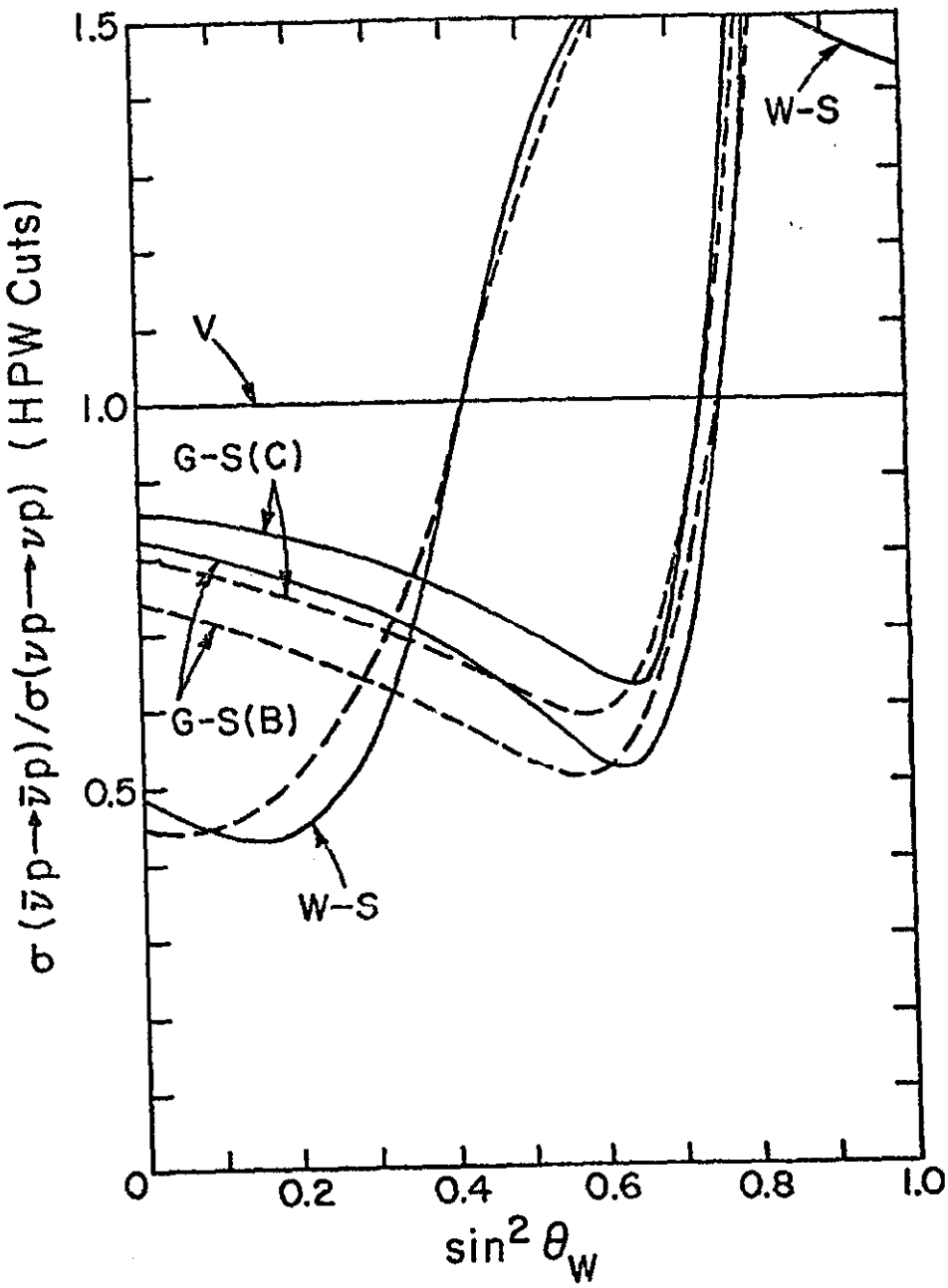
1.5
1.0
0.5
0
0.2
0.4
0.6
0.8
1.0
$\sin^2\theta_W$
$\sigma(\bar{\nu}p\to\bar{\nu}p)/\sigma(\nu p\to\nu p)$ (HPW Cuts)
V
G-S(C)
G-S(B)
W-S
W-S

Fig. 25